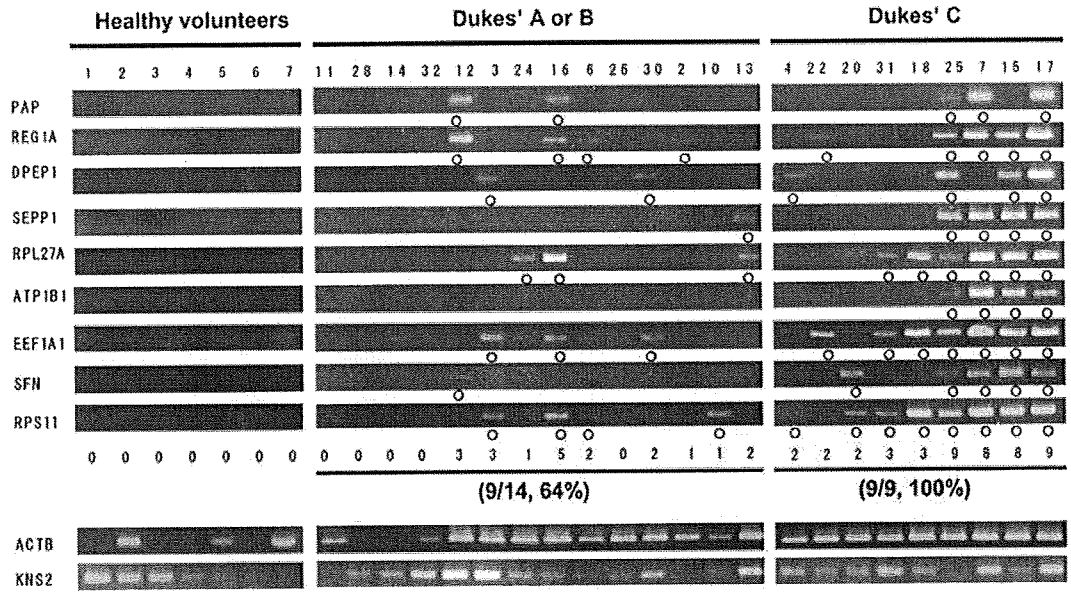

Figure 2. Results of RT-PCR of 9 genes (PAP, REG1A, DPEEP1, SEPP1, RPL27A, ATP1B1, EEF1A1, SFN, and RPS11) in the colonocyte RNA samples from 23 curable colorectal cancer patients and 7 healthy volunteers. We performed RT-PCR of the first 3 identified genes (PAP, REG1A, and DPEP1) in the colonocyte RNA samples which were prepared from 23 curable colorectal cancer patients (8 Dukes stage A, 6 Dukes stage B, and 9 Dukes stage C) and 7 healthy volunteers. Next, to test the power of the 85 genes, which were identified by colonocyte gene expression profiling, we randomly selected 6 (SEPP1, RPL27A, ATP1B1, EEF1A1, SFN, and RPS11), and performed RT-PCR on the same samples. In total, RT-PCR of those 9 genes detected 18 (78%) of the 23 cancer patients, and 9 (64%) of the 14 early cancers (Dukes stage A or B) were detected; however, the expression of all of the 7 genes was hardly detected in the 7 healthy volunteers (upper panel). The expression level of housekeeping genes such as ACTB (ß-actin) was highly varied from sample to sample (lower panel). KNS2 encoding kinesin 2 was selected, by microarray analyses, as a gene expressed constantly in any colonocyte RNA sample; however, the expression level was also varied. Open circles indicate positive RT-PCR product, and numbers indicate the number of the positive genes in each sample.

with Dukes stage A, 6 with Dukes stage B, and 9 with Dukes stage C cancers; 5 were right-sided and 18 were left-sided cancers. Twelve (52%) of the 23 cancers were positive by RT-PCR in at least one of the 3 genes whereas no positive gene was found in any of the healthy volunteers (Fig. 2). To test the power of the 85 genes, which were identified by colonocyte gene expression profiling, we randomly selected 6 (SEPP1, RPL27A, ATP1B1, EEF1A1, SFN, and RPS11). RT-PCR of these 6 genes detected 16 (70%) of the 23 cancers as at least positive for 1 gene whereas no positive gene was found in any of the healthy volunteers (Fig. 2). No or a quite low signal of all the 9 genes was found in another RT-PCR experiment with 8 healthy volunteers (data not shown). In total, RT-PCR of those 9 genes detected 18 (78%) of the 23 cancer patients (Fig. 2). The 18 patients detected were 4 with Dukes stage A, 5 with Dukes stage B, and 9 with Dukes stage C cancers; 4 were right-sided and 14 were left-sided cancers. Therefore, 9 (64%) of the 14 early cancers (Dukes stage A or B), which have no lymph node metastasis, and show a good prognosis, were able to be detected. Importantly, 4/5 (80%) of the right-sided colorectal cancers were detected, which have been reported to be very difficult to detect by any feces-based molecular biological method, because most right-sided cancer-derived colonocytes are severely damaged from remaining for a long time in the feces.

For fecal RNA-based detection of early colorectal cancer, quantitative real-time RT-PCR is thought to hardly apply in the colonocyte because the expression level of housekeeping genes was highly varied from sample to sample (Fig. 2). The expressional variation could be explained by the difference of the physiological condition of colorectal cancer cells and anal squamous cells isolated from the feces by FMCI. All of the 9 genes were selected as cancer cell- or cancer patient-derived colonocyte-specific genes. Therefore, a negative or positive assay was thought to be sufficient for fecal RNA-based colorectal cancer detection. Accordingly, we developed a multiplex RT-PCR-based microarray assay for evaluating the above RT-PCR results and for providing an effective imaging tool for mass cancer screenings (Fig. 3). The Cy3-labeled cDNAs prepared by multiplex RT-PCR in a single tube were hybridized with 9 gene sequences on a focused microarray, which was manufactured by our previously developed Bubble Jet Technology with a small modification (25). Hybridization signals and the number of positive genes in the above 23 cancer patient-derived colonocyte RNA samples and 7 healthy volunteer-derived colonocyte RNA samples are shown in Fig 4. In total, a high concordance was observed between the focused microarray and RT-PCR. The focused microarray detected 18 (78%) of the 23 cancer patients. Ten (71%) of the 14 early cancers (Dukes stage A or B) and 4 (80%) of the 5 right-sided cancers were detected.

Discussion

Although the number of samples examined in this study is considered to be small, the evidence suggests that these successful results could be obtained from the high-quality of the RNA of the colonocytes, which were isolated by FMCI. From a practical point of view for mass cancer screenings, it is noted that the same number of colonocytes from fecal

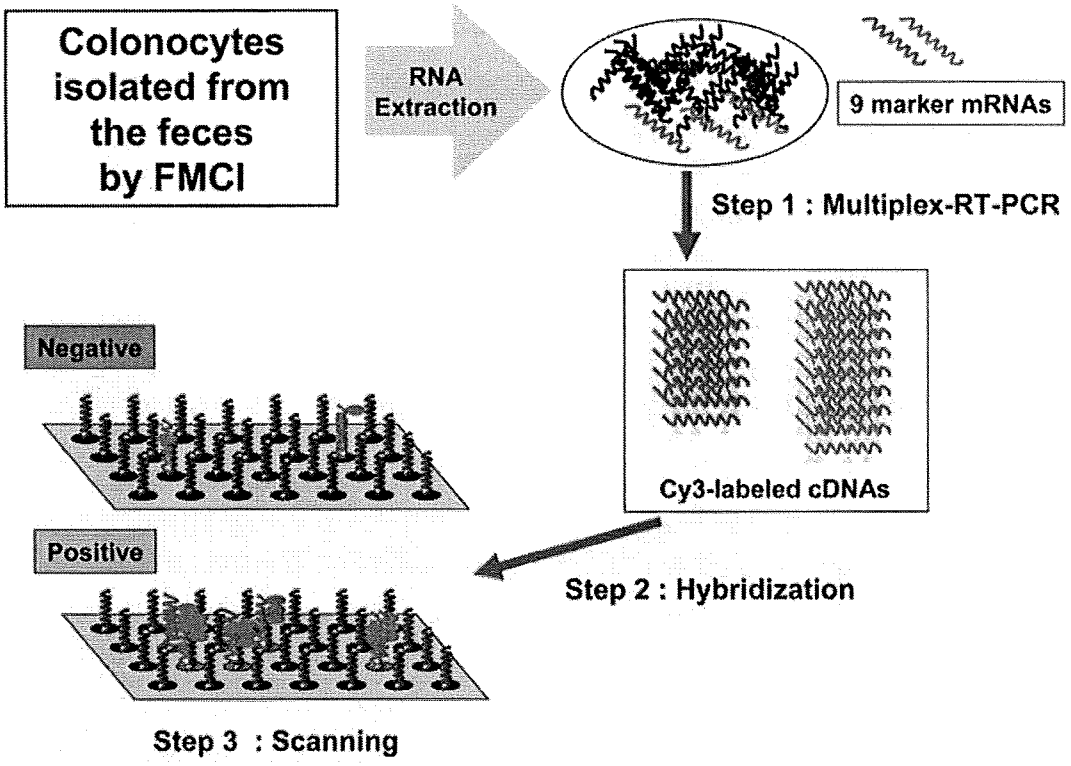

Figure 3. Schematic flow diagram of a focused micoarray assay. Marker mRNAs (PAP, REG1A, DPEP1, SEPP1, RPL27A, ATP1B1, EEF1A1, SFN, and RPS11 mRNAs) were amplified and labeled with Cy3-dUTP by multiplex-RT-PCR among total RNAs from colonocytes isolated by FMCI (step 1) and hybridized to focused micoarray (step 2), followed by fluorescence intensity scanning (step 3).

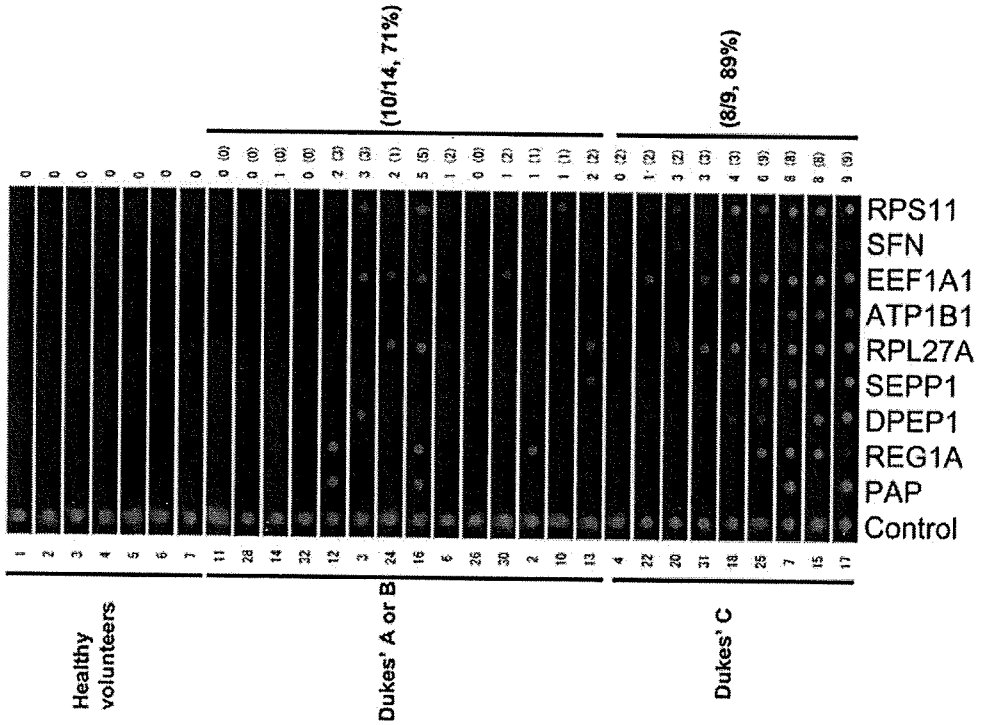

Figure 4. Hybridization image of focused microarray analysis and the number of positive genes in 30 colonocyte RNA samples. The Cy3-labeled cDNAs prepared by multiplex RT-PCR in two tubes were hybridized with 9 gene sequences (PAP, REG1A, DPEP1, SEPP1, RPL27A, ATP1B1, EEF1A1, SFN, and RPS11) on a focused microarray, which was manufactured by our previously developed Bubble Jet Technology with a small modification (25). Hybridization signals and the number of positive genes (right) in the above 23 cancer patient-derived colonocyte RNA samples and 7 healthy volunteer-derived colonocyte RNA samples are shown. In total, a high concordance was observed between focused microarray and RT-PCR. Ten (71%) of the 14 early cancers (Dukes stage A or B) and 8 (89%) of 9 Dukes stage C cancers were detected by the focused microarray analysis. The number of positive genes in RT-PCR are in parentheses (Fig. 2).

materials 6 h to 3 days after evacuation can be obtained if the feces are kept at 4˚C (23). However, if conventional fecal RNA preparation methods without the epithelial cell enrichment process are used for colorectal cancer screening, we have to consider the contamination of blood in the feces, which derives from nonmalignant diseases. Considering the use of such methods, to this end we further provided 56 genes, which were expressed in the cancer patient-derived colonocytes but not in either the healthy volunteer-derived colonocytes or the peripheral blood mixture (Table II). This study suggests that the fecal RNA-based method could be a promising procedure for the detection of early or right-sided colorectal cancers. We recently developed a very effective focused microarray assay for detecting minimal gastric cancer cells in peritoneal washings, demonstrating a specificity and sensitivity equal to or better than cytology in two large specialist hospitals with trained cytologists (26). Therefore, the focused microarray assay could provide an effective imaging tool for mass screening, and our extensive gene list provides useful markers.

Acknowledgments

This study was supported in part by the program for promotion of Fundamental Studies in Health Sciences of the National Institute of Biomedical Innovation (NiBio); in part by a Grant-in-Aid for the Third Comprehensive 10-Year Strategy for Cancer Control and for Cancer Research (16-15) from the Ministry of Health, Labour and Welfare of Japan, and in part by a research and development project of the Industrial Science and Technology Program supported by the New Energy and Industrial Technology Development Organization (NEDO) of Japan. We thank Ayako Nomura and Megumi Sato for their excellent assistance with primer design for RT-PCR.

References

1. Mandel JS, Bond JH, Church TR, Snover DC, Bradley GM, Schman LM and Ederer F: Reducing mortality from colorectal cancer by screening for fecal occult blood. Minnesota Colon Cancer Control Study. N Engl J Med 328: 1365-1371, 1993.
2. Hardcastle JD, Chamberlain JO, Robinson MH, Moss SM, Amar SS, Balfour TW, James PD and Mangham CM: Randomised controlled trial of faecal-occult-blood screening for colorectal cancer. Lancet 348: 1472-1477, 1996.
3. Kronborg O, Fenger C, Olson J, Jorgensen OD and Sondergaard O: Randomized study of screening for colorectal cancer with faecal-occult-blood test. Lancet 348: 1467-1471, 1996.
4. Towler B, Irwig L, Glasziou P, Kewenter J, Weller D and Silagy C: A systematic review of the effects of screening for colorectal cancer using the faecal occult blood test, hemoccult. BMJ 317: 559-565, 1998.
5. Winawer S, Fletcher R, Rex D, Bond J, Burt R, Ferucci J, Ganiats T, Levin T, Woolf S, Johnson D, Kirk L, Litin S and Simmang C: Colorectal cancer screening and surveillance: clinical guidelines and rationale-update based on new evidence. Gastroenterology 124: 544-560, 2003.
6. Mandel JS, Church TR, Bond JH, Ederer F, Geisser MS, Mongin SJ, Snover DC and Schuman LM: The effect of fecal occult-blood screening on the incidence of colorectal cancer. N Engl J Med 343: 1603-1607, 2000.
7. Sidransky D, Tokino T, Hamilton SR, Kinzler KW, Levin B, Frost P and Vogelstein B: Identification of ras oncogene mutations in the stool of patients with curable colorectal tumors. Science 256: 102-105, 1992.
8. Hasegawa Y, Takeda S, Ichii S, Koizumi K, Maruyama M, Fujii A, Ohta H, Nakajima T, Okuda M, Baba S, *et al*: Detection of K-ras mutations in DNAs isolated from feces of patients with colorectal tumors by mutant-allele-specific amplification (MASA). Oncogene 10: 1441-1445, 1995.
9. Smith-Ravin J, England J, Talbot IC and Bodmer W: Detection of c-Ki-ras mutations in faecal samples from sporadic colorectal cancer patients. Gut 36: 81-86, 1995.
10. Eguchi S, Kohara N, Komuta K and Kanematsu T: Mutations of the p53 gene in the stool of patients with resectable colorectal cancer. Cancer 77: 1707-1710, 1996.
11. Nollau P, Moser C, Weinland G and Wagener C: Detection of K-ras mutations in stools of patients with colorectal cancer by mutant-enriched PCR. Int J Cancer 66: 332-336, 1996.
12. Ratto C, Flamini G, Sofo L, Nusera P, Ippliti M, Curigliano G, Ferreti G, Sgambato A, Merico M, Doglietto GB, Cittadini A and Crucitti F: Detection of oncogene mutation from neoplastic colonic cells exfoliated in feces. Dis Colon Rectum 39: 1238-1244, 1996.
13. Deuter R and Muller O: Detection of APC mutations in stool DNA of patients with colorectal cancer by HD-PCR. Hum Mutat 11: 84-89, 1998.
14. Ahlquist DA, Skoletsky JE, Boynton KA, Harrington JJ, Mahoney DW, Pierceall WE, Thibodeau SN and Shuber AP: Colorectal cancer screening by detection of altered human DNA in stool: feasibility of a multitarget assay panel. Gastroenterology 119: 1219-1227, 2000.
15. Dong SM, Traverso G, Johnson C, Geng L, Favis R, Boynton K, Hibi K, Goodman SN, D'Allessio M, Paty P, Hamilton SR, Sidransky D, Barany F, Levin B, Shuber A, Kinzler KW, Vogelstein B and Jen J: Detecting colorectal cancer in stool with the use of multiple genetic targets. J Natl Cancer Inst 93: 858-865, 2001.
16. Rengucci C, Maiolo P, Saragoni L, Zoli W, Amadori D and Calistri D: Multiple detection of genetic alterations in tumors and stool. Clin Cancer Res 7: 590-593, 2001.
17. Traverso G, Shuber A, Olsson L, Levin B, Johnson C, Hamilton SR, Boynton K, Kinzler KW and Vogelstein B: Detection of proximal colorectal cancers through analysis of faecal DNA. Lancet 359: 403-404, 2002.
18. Traverso G, Shuber A, Levin B, Levin B, Johnson C, Hamilton SR, Boynton K, Kinzler KW and Vogelstein B: Detection of APC mutations in fecal DNA from patients with colorectal tumors. N Engl J Med 346: 311-320, 2002.
19. Boynton KA, Summerhayes IC, Ahlquist DA and Shuber AP: DNA integrity as a potential marker for stool-based detection of colorectal cancer. Clin Chem 49: 1058-1065, 2003.
20. Matsumura Y and Tarin D: Significance of CD44 gene products for cancer diagnosis and disease evaluation. Lancet 340: 1053-1058, 1992.
21. Mastumura Y, Hanbury D, Smith J and Tarin D: Non-invasive detection of malignancy by identification of unusual CD44 gene activity in exfoliated cancer cells. BMJ 308: 619-624, 1994.
22. Yamao T, Matsumura Y, Shimada Y, Moriya Y, Sugihara K, Akasu T, Fujita S and Kakizoe T: Abnormal expression of CD44 variants in the exfoliated cells in the feces of patients with colorectal cancer. Gastroenterology 114: 1196-1205, 1998.
23. Matsushita H, Matsumura Y, Moriya Y, Akasu T, Fujita S, Yamamoto S, Onouchi S, Saito N, Sugito M, Ito M, Kozu T, Minowa T, Nomura S, Tsunoda H and Kakizoe T: A new method for isolating colonocytes from naturally evacuated feces and its clinical application to colorectal cancer diagnosis. Gastroenterology 129: 1918-1927, 2005.
24. Mori K, Aoyagi K, Ueda T, Danjoh I, Tsubosa Y, Yanagihara K, Matsuno Y, Sasako M, Sakamoto H, Mafune K, Kaminishi M, Yoshida T, Terada M and Sasaki H: Highly specific marker genes for detecting minimal gastric cancer cells in cytology negative peritoneal washings. Biochem Biophys Res Commun 313: 931-937, 2004.
25. Okamoto T, Suzuki T and Yamamoto N: Microarray fabrication with covalent attachment of DNA using Bubble Jet Technology. Nat Biotech 18: 438-441, 2000.
26. Mori K, Suzuki T, Uozaki H, Nakanishi H, Ueda T, Matsuno Y, Kodera Y, Sakamoto H, Yamamoto N, Sasako M, Kaminishi M and Sasaki H: Detection of minimal gastric cancer cells in peritoneal washings by focused microarray analysis with multiple markers: clinical implications. Ann Surg Oncol 14: 1694-1702, 2007.

Available online at www.sciencedirect.com
ScienceDirect
Journal of Controlled Release 117 (2007) 267–272
journal of controlled release
www.elsevier.com/locate/jconrel
GENE DELIVERY

Spinal gene transfer using ultrasound and microbubbles

Masahiko Takahashi [a,*], Kanta Kido [a], Atsuko Aoi [a,b], Hiroshi Furukawa [c], Masao Ono [c], Tetsuya Kodama [b]

[a] *Department of Oral Medicine and Surgery, Tohoku University Graduate School of Dentistry, Japan*
[b] *Department of Nanomedicine, Tohoku University Biomedical Engineering Research Organization, Japan*
[c] *Department of Pathology, Tohoku University Graduate School of Medicine, Japan*

Received 19 June 2006; accepted 24 October 2006
Available online 6 November 2006

Abstract

Spinal gene therapy is a promising option for treating various spinal-related disorders. Several previous studies using viral vectors reported successful transfer of therapeutic genes into the spinal nerve system. However, because of the considerable immunogenicity related to the use of viruses, non-viral gene transfer still needs to be developed. One possible approach is the combined use of ultrasound and echo-contrast microbubbles. The present study shows that this method can be applied for targeted intrathecal gene delivery. We intrathecally injected a mixture of plasmid-DNA encoded with luciferase and commercially available albumin microbubbles by needle puncture at the lower lumbar intervertebral space in mice. Subsequent percutaneous ultrasonication on the lumbar vertebrae significantly enhanced the luciferase expression, analyzed by imaging luciferin bioluminescence, in the dorsal meningeal cells at the insonated region. No apparent neurological damages were induced by the present spinal interventions. In addition to the general benefits of the combined use of ultrasound and microbubbles, our approach can offer some advantages specific to spinal gene transfection including minimal invasiveness of simple percutaneous dural puncture, targetability due to the limited access of ultrasound waves through anatomical apertures of the vertebrae, and possible paracrine delivery of therapeutic molecules to the spinal nerve system.

Keywords: Gene therapy; Spinal disorder; Intrathecal delivery; Ultrasound; Microbubble

1. Introduction

Spinal gene transfer is expected to become a promising option for treating various spinal-related disorders including nerve injury, degenerative diseases, neoplasm, and chronic pain [1,2]. To date, the most widely used vehicles for gene delivery are viral vectors. Recent animal studies using adenovirus vectors indicated that direct spinal injection of specific growth-factor genes achieved functional recovery after acute spinal cord injury [3–5]. The feasibility of virus-mediated gene transfer to treat chronic pain has been also explored using the precursor genes of endogenous opioids [6,7]. The targeted spinal tissues for the opioid-gene transfer can be both meningeal and parenchyma cells. Among the utilized viral vectors that are mostly derived either from adenoviruses, adeno-associated viruses, herpes simplex viruses or retroviruses [8], herpes vectors may be the most promising for antinociceptive gene therapy because of its high selectivity to primary afferent neurons [2,9].

Despite such experimental successes in virus-mediated gene delivery, however, alternative non-viral transgene applications need to be developed because the clinical use of viral vectors is limited by such possible disadvantages as immunogenic properties, inflammatory responses, and the difficulty of producing large amounts of pure virus. In this context, it has been reported recently that the emission of high-pressure ultrasound in combination with echo-contrast agents, microbubbles, can facilitate gene transfection into cells [10]. Possible explanations for the mechanisms include the production of transient pores on the cell membranes as well as an increase in the

* Corresponding author. Division of Dento-oral Anesthesiology, Department of Oral Medicine and Surgery, Tohoku University Graduate School of Dentistry, 4-1 Seiryo-machi, Aoba-ku, Sendai 980-8575, Japan. Tel./fax: +81 22 717 8401.
E-mail address: m-takaha@mail.tains.tohoku.ac.jp (M. Takahashi).

0168-3659/$ - see front matter © 2006 Elsevier B.V. All rights reserved.
doi:10.1016/j.jconrel.2006.10.026

membrane fluidity by impulsive pressures raised when microbubbles are disrupted by ultrasound [11,12]. The combined use of microbubbles and ultrasound for gene delivery has several advantages including low toxicity, low immunogenicity, low invasiveness, high target selectivity, and repeatable applicability [11]. In the present study, we focused on spinal gene delivery and demonstrated that percutaneous ultrasonication in combination with intrathecal microbubbles facilitated gene transfection in spinal meningeal cells in mice.

2. Materials and methods

2.1. Animals

The study was approved by the Animal Care Committee of Tohoku University Graduate School of Medicine. Male inbred BALB/c mice were purchased from the institutional breeding facilities at 5–6 weeks of age and maintained in an antigen- and virus-free room (22±1 °C, 60±10% relative humidity, 12 h/12 h light/dark cycle, food and water *ad libitum*). The mice were studied at 7–8 weeks of age.

2.2. Plasmid DNA

pCMV-luciferase-GL3 (pcLuc-GL3: 7.4 kb) was constructed by cloning the luciferase gene from the pGL3-Control Vector (Promega Corp., Madison, WI, USA) into pcDNA3 (5.4 kb) (Invitrogen, San Diego, CA, USA) at the *Hin*dIII and *Bam*HI sites. Plasmid DNA was purified with a QIAGEN plasmid isolation kit (QIAGEN, Hilden, Germany) and prepared at a final concentration of 1 mg/ml.

2.3. Intrathecal transfection of plasmid DNA

Mice were anesthetized with an intraperitoneal injection of sodium pentobarbital (80 mg/kg) and immobilized in a prone position on an acrylic plate. Intrathecal access was accomplished by percutaneous lumbar puncture through the 4/5th or 5/6th intervertebral space using a 27-gauge stainless-steel needle according to the Hylden and Wilcox technique with modification [13]. Dural penetration of the needle was confirmed by inspecting tail flicks of the mice. A total volume of 10 μl containing 5 μg plasmid and commercially available albumin-coated octa-fluoropropane gas microbubbles (MB), Optison™ (Amersham Health, Oslo, Norway; $5–8\times10^8$/ml, 3–4.5 μm in diameter), in phosphate buffered saline at a final MB concentration either 0, 20, or 50 v/v% was then injected slowly into the intrathecal space using a 50-μl microsyringe (Hamilton, Bonaduz, GR, Switzerland). A mixture of the plasmid with MB was prepared by gentle hand shaking immediately before injection. Immediately after the intrathecal injection, the mice were placed at a vertical position in a 37 °C water bath and dorsally insonated for 1 min at the vertebral region that had been injected using an ultrasound-emitting transducer (6 mm in diameter; Fuji Ceramics Co., Fujinomiya, Japan). The ultrasound (US) parameters used were as follows: central frequency, 950 kHz; duty ratio, 20%; the average intensity per cross section, 1.3 W/cm^2; acoustic pressure at a standoff distance of 1 mm from the transducer surface, 0.6 MPa; energy, 2.4 J/cm^2. After the insonation, the mice were dried and kept under a heat lamp until recovery from anesthesia.

2.4. Analysis of luciferase activity

Mice were killed by neck dislocation under deep anesthesia with isoflurane at 1, 3, 7 days after transfection of the luciferase gene. The spinal cord was harvested *en bloc* at the level of the lower thoracic to sacral region by careful dissection of the vertebrae and placed on a dish plate. Subsequently, the tissue was fully covered with Luciferin 30 mg in 1 ml PBS (Promega Co., Madison, WI, USA). Luciferin bioluminescence was immediately quantified as the luciferase activity using an *in vivo* imaging system (IVIS™, Xenogen Co., Alameda, CA, USA) [14].

2.5. Immunohistochemistry

The harvested spinal cords were preserved in 10% PFA for 4 h and then embedded in paraffin and sectioned. Sections (4 μm thickness) were evaluated for the presence of luciferase protein by immunostaining. The sections were deparaffinized in xylene for 5 min 3×, rehydrated through graded ethanol and equilibrated in PBS. The sections were incubated in 3% H_2O_2 for 30 min to dampen endogenous peroxidase activity. They were incubated for 30 min at room temperature with 10% normal goat serum (Nichirei Biosciences Inc., Tokyo) to reduce nonspecific protein binding. After a wash in PBS, the sections were incubated with biotin-labeled rabbit anti-luciferase antibody (0.5 g/ml) (Cortex Biochem, San Leandro, CA, USA) overnight at 4 °C. The following day, after three washes in PBS, immunoreactivity was detected using an anti-rabbit IgG Histofine SAB-PO(M) kit (Nichirei Biosciences Inc., Tokyo, Japan) and diaminobenzidine (DAB) as a chromogen according to the manufacturer's protocols. After color development, the spinal cord sections were counterstained with hematoxylin and were then dehydrated, cleared, and mounted on slides.

2.6. Assessment of post-transfectional spinal injury

2.6.1. Thermal nociception

For assessing the nociceptive responses to thermal stimuli after the intrathecal procedure, the paw withdrawal latencies following exposure to infra-red radiant heat were determined [15] using a commercial device (7370-Planter Test, Ugo Basille, Comerio, Italy) three days after the gene transfection. Mice were placed in a clear plastic chamber (210 mm × 105 mm × 130 mm) with a glass floor and allowed to acclimate for at least 5 min. After the acclimation period, radiant heat was projected to the hind paw and time count was started. The heat projection was made through a 5 mm × 10 mm aperture in the top of a movable case containing the radiant heat source that was positioned under the glass floor directly beneath the paw. The radiant heat source consisted of a high intensity projecting Halogen lamp bulb (8 V–50 W) located 40 mm below the floor. The time count was stopped when the mouse withdrew its paw. Mice were tested

with three determinations each at the right and left paw and were allowed to rest for at least 30 min between each session.

2.6.2. Rotarod

For assessing motor function after the intrathecal procedure, mice were tested using a rotarod (IITC; Life Science Instrument, Woodland Hills, CA, USA) three days after the gene transfection. The rod had a diameter of 3.8 cm and was accelerated from 0 to 30 rpm over a 17.5-s period. The total time that the mice remained on the rotarod was measured. The time count was stopped when mice fell from the rod or when they rotated around completely two times without walking [16]. Mice were tested with three trials and were allowed to rest for at least 30 min between each session.

2.7. Statistical analysis

All values are expressed as mean±SEM. Statistical analysis for the spinal luciferase activities was performed by one-factor analysis of variance (ANOVA) with Fisher's protected least significant difference test (Fisher's PLSD) as a post-hoc procedure. Unpaired Student-T test was used for the behavioral evaluations. Statistical significance was defined as $p<0.05$.

3. Results

3.1. Effects of microbubbles and ultrasound on spinal gene transfection

Fig. 1 shows representative views of luciferin bioluminescence in the mouse spinal cord obtained by the imaging system (sum of photon counts from a region of interest at 5 min is presented). The spinal luciferase activities determined one day after four different treatments (DNA alone, DNA+MB, DNA+US, and DNA+MB+US) are shown in Fig. 2a. The concentration of MB used was 50%. The luciferase activities in the treatments with DNA+MB and DNA+US were as low as that with DNA alone. In contrast, ultrasonication after the DNA+MB injection significantly increased the luciferase activity by approximately 25 fold compared to the other treatments ($p<0.001$).

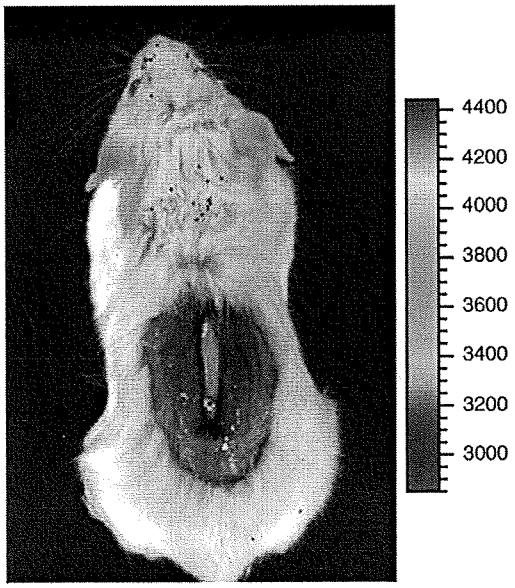

Fig. 1. Representative image showing luciferin bioluminescence (IVIS™, Xenogen Co., Alameda, CA, USA) in the spinal cord of BALB/c mice a day after the intrathecal injection of plasmid DNA and microbubbles (Optison™, Amersham Health, Oslo, Norway) followed by percutaneous ultrasonication. Imaging time is 5 min. Color bar units represent photons s^{-1} cm^{-2}.

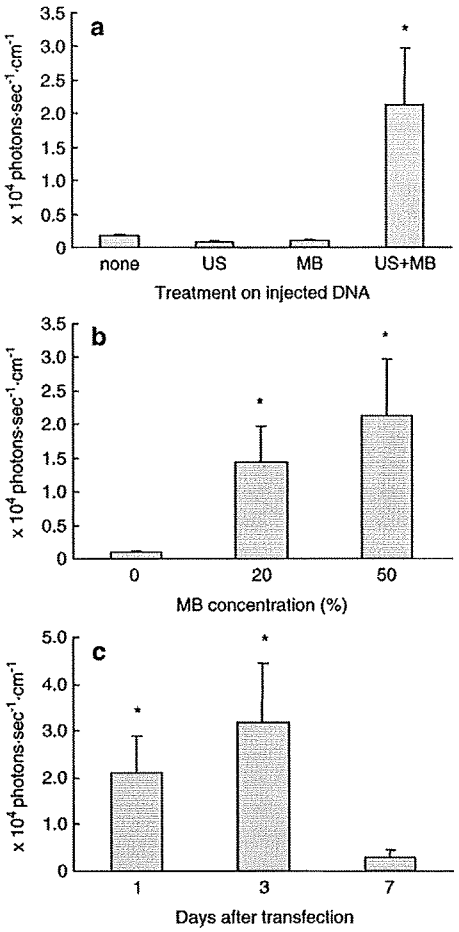

Fig. 2. Plasmid-derived spinal luciferase activity represented by luciferin bioluminescence in mice subjected to intrathecal gene delivery using ultrasound and microbubbles. The ultrasound parameters were as follows: central frequency, 950 kHz; duty ratio, 20%; the average intensity per cross section, 1.3 W/cm^2; acoustic pressure at a standoff distance of 1-mm from the transducer surface, 0.6 MPa; energy, 2.4 J/cm^2; exposure time, 1 min. (a) Treatment effects of ultrasound and 50% microbubbles one day after the application. Combined use of ultrasound and microbubbles significantly enhanced the gene transfection compared to the other treatments. (b) Effects of the microbubble concentration on the spinal gene expression. Microbubbles at concentrations of both 20 and 50% significantly enhanced the gene transfection one day after the application. No significant difference was found between the luciferase activities in mice treated with the two concentrations. (c) Time course of spinal gene expression in mice treated with ultrasound and 50% microbubbles. Luciferase activity significantly increased at 1 and 3 days after gene transfection which disappeared by the 7th day. No statistical difference was found between the gene expression at 1 and 3 days post-transfection. *$p<0.001$. $n=5$ in each group. US: ultrasound; MB: microbubble (Optison).

3.2. Effects of microbubble concentration on spinal gene transfection

Fig. 2b shows the spinal luciferase activities one day after ultrasonication with 0, 20, and 50% MB. While the treatment with MB significantly increased the luciferase activities ($p<0.02$), the difference between 20 and 50% MB was not significant.

3.3. Time course of spinal gene expression

The spinal luciferase activities were analyzed at 1, 3, and 7 days after the intrathecal gene transfection using US and 50% MB (Fig. 2c). The luciferase activities significantly increased at 1 and 3 days post-transfection ($p<0.02$) without an intergroup difference, and returned to a level similar to that without US (at 1 day post-treatment) after 7 days.

3.4. Histological localization of the transfected gene expression

The immunohistochemical staining revealed that luciferase expression was mostly limited to the meningeal cells in the dorsal surface of the spinal cord (Fig. 3). The expressing regions were likely to have been the dura mater because Fig. 3b clearly shows a positive staining for cells in a membrane structure apart from the spinal parenchyma by the space of medullary fluid. As the dura mater consists of two cell types, meningeal cell and endothelial cell, the present data cannot strictly exclude the positive staining for the endothelial cells. However, the endothelial cells are shown to be very minor cellular component, so that frequent staining may indicate expression of the gene product mainly in the meningeal cells. There were no hemorrhage or inflammatory findings in the sections.

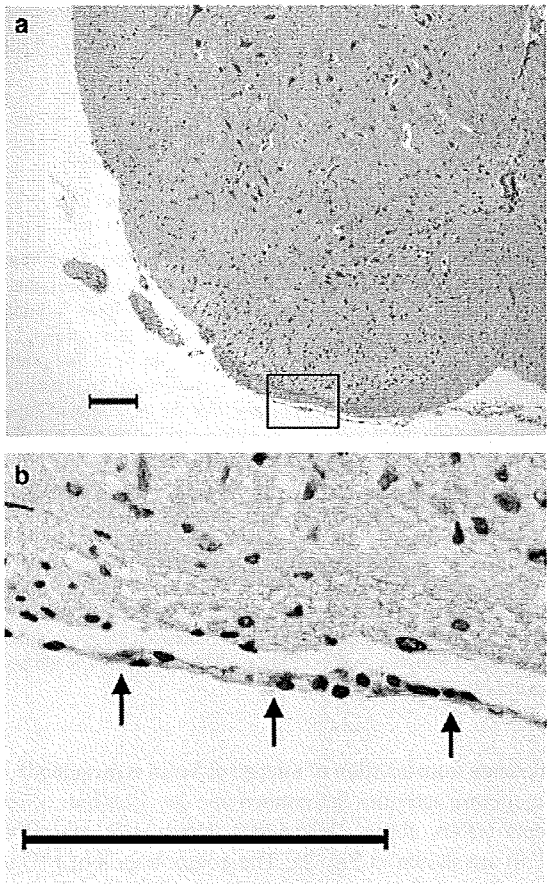

Fig. 3. Local gene expression in mouse spinal cord after intrathecal gene delivery using ultrasound and microbubbles. Expression of luciferase protein was mostly limited to the dorsal meningeal cells. (a) H&E staining in coronal sections of the lumber spinal cord. (b) Immunohistochemical localization of luciferase (arrows). Scale bar=100 μm.

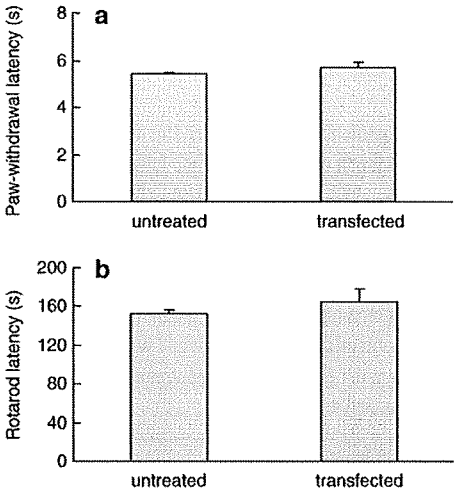

Fig. 4. Neurological evaluations of mice obtained 3 days after gene transfection using ultrasound and microbubbles (50%). (a) Paw-withdrawal latency following exposure to infra-red radiant heat. Three determinations each in the right and left hind paw were combined in each animal because the latency did not differ between the two sides. (b) Rotarod latency that represents the total time mice remained on the rotarod. Each mouse was tested with three trials. No significant difference was found compared to untreated mice in either determination. $n=4$ in each group. US: ultrasound; MB: microbubble (Optison).

3.5. Paw-withdrawal and rotarod latencies

Fig. 4 shows the averaged paw-withdrawal (Fig. 4a) and rotarod latencies (Fig. 4b) in untreated and transfected (DNA+50% MB+US) mice. Since the withdrawal latencies were not different between the right and left paw (data not shown), the data were combined in each animal. The determinations revealed no significant difference in the paw-withdrawal or rotarod latencies between the two groups, indicating that the present intervention did not affect the sensory and motor neurologic functions of the mice.

4. Discussion

The present study clearly demonstrated that percutaneous ultrasonication on an intrathecally administered mixture of plasmid-DNA and Optison facilitated the transfection of luciferase genes into the spinal meningeal cells in mice. No significant deficit was observed either in the sensory or motor neurologic functions after the procedures. In addition to the

general benefits of the combined use of ultrasound and microbubbles, our approach offers some advantages specific to spinal gene transfection. First, it requires only intrathecal needle access and percutaneous sonication that have been widely accepted in the clinical practice. Although a relatively short duration of gene expression (<7 days) was observed (Fig. 2c), the minimal invasiveness of the present surgical interventions would permit repetitive gene delivery into the spinal cord. Second, the intervertebral foramina and spaces would provide highly selective anatomical windows for ultrasound access while the vertebral bony structures would protect the spinal cord from possible excessive sonication. Although spotty gene expressions in the insonated regions would not be obvious in animals as small as the mice used in this study (Fig. 1), it can be expected that an ultrasound beam could reach the regions of the dorsal roots or the dorsal horns at targeted vertebral levels through the boneless apertures in large animals including human. This can be especially promising for transferring antinociceptive genes. Third, gene transfer into meningeal cells (Fig. 3) may be useful for topical delivery of bioactive substances into the CSF or adjacent spinal parenchyma while avoiding direct genetic modulation of parenchyma cells. Transgene-derived peptides such as growth factors, neuropeptides, or endogenous opioids that are secreted from meningeal cells would act in a paracrine manner on neurons and glias in the near vicinity, circumventing pharmacological problems related to the short half-life of the peptides or the need for high doses to achieve biological activity that could result in undesirable side effects.

Spinal gene therapy can be expected to be a promising approach to treat various spinal-related disorders. In previous animal studies, the delivery of therapeutic genes into the spinal nerve system has been mostly achieved using viral vectors [8]. However, because of the considerable disadvantages involved in using viral vectors, the development of alternative non-viral transgene techniques is needed. Cationic reagents such as cationic liposomes [17] have been developed for non-viral gene transfection. Achieving the efficient delivery of such molecules, however, to the spinal cord includes inherent difficulties. First, intrathecal injection induces diffusion of reagents into the cerebral spinal fluid (CSF), resulting in lack of target specificity. Second, since the CSF continuously circulates and replaces, a constant concentration of reagents for necessary transfection to a specific site would not be achieved. Ultrasound gene therapy is an alternative non-viral approach [18]. The insufficient transfection efficiency of simple ultrasonication can be improved by the combined use of echo-contrast microbubbles [11]. The use of ultrasound with microbubbles, which enables non-invasive, tissue-specific gene delivery, has received much interest and enhanced gene transfer has been reported in various animal tissues *in vivo* including heart [19], peripheral arteries [20], skeletal muscles [21], and brain [22]. Very recently, Shimamura et al. reported successful gene transfer into the rat spinal cord using ultrasound and microbubbles [23]. The authors intrathecally injected naked luciferase DNA with Optison through the 4/5th lumbar intervertebral space and applied sonication directly on the thoracic dural sac by removing the dorsal part of the 9–10th thoracic vertebra, which resulted in the enhanced expression of luciferase in the meningeal cells in the insonated region. In contrast, we accomplished transgene expression in the meningeal cells by intrathecal injection of luciferase DNA with Optison through the lower lumbar intervertebral space, as in their study, but then employed simple transcutaneous insonation at the same lumbar region without surgical exposure of the dura. The lower invasiveness in our methodology would seem to be more clinically useful. Interestingly, the duration of transgene expression was consistently as short as a week in both studies. Although Shimamura et al. described that the short expression of transgene by single transfection would be acceptable to treat acute spinal cord trauma [23], the repeated applicability due to the lower invasiveness in the present study could enable treatments for chronic ailments. In fact, we have recently shown that successive gene expression was obtained by repeat transfection using the present ultrasound–microbubble technique [24]. Nonetheless, since gene expression for longer than 3 weeks was previously achieved by spinal electroporation via an intrathecal electrode catheter in rat meningeal cells [25,26], the present ultrasound–microbubble approach has the potential for methodological improvement to prolong the duration of transgene expression by optimizing acoustic parameters such as intensity, duty ratio, frequency, and spatial pressure distribution [12] and changing the membrane properties of microbubbles [27].

The present acoustic parameters were relatively consistent with those reported in previous studies in which ultrasound and Optison were safely used for transferring genes into nervous tissues [22,23]. Consistent with those studies, we did not find macroscopic injuries in the skin or muscles, microscopic damage in the spinal cord, or significant deficits in the spinal neurological functions. In addition, the present neurological tolerance may be alternatively explained by a characteristic of our approach, namely that the intact vertebral bony structures surrounding the intervertebral apertures limited excessive sonication of the spinal cord. Nonetheless, further optimization of the ultrasound parameters will improve the safeness of sonication on nervous tissues. The physical conditions of the microbubbles used in this study are additional issues to be discussed. First, although we evaluated only the usefulness of Optison, the possible utility and safety of microbubbles other than Optison (e.g. lipid microbubbles) for intrathecal gene transfer remains to be explored. Second, we should note that Optison at a concentration as high as 50% was used in most series of the present experiments. The reasons for this were that a trend of higher transfection efficacy was observed in the 50% group (but ns vs. 20% groups, Fig. 2b) and that no apparent neurological damage was observed in the transfected mice (Fig. 4). However, earlier studies [22,23] successfully used Optison at concentrations of 20–25% for intrathecal gene delivery in rats. It seems reasonable that intrathecal microbubbles at lower concentrations would induce fewer adverse effects while enabling an increase in the relative content of plasmid DNA in a limited volume of mixture. Therefore, it is possible that the concentration of microbubbles for intrathecal injection could be further optimized. The authors finally note

that the functional expressions of genes transfected into the spinal nerve system have not yet been examined. Further efforts using genes that are encoded with neurobioactive peptides are clearly needed to investigate the clinical usefulness of the present ultrasound–microbubble approach.

In conclusion, we demonstrated that simple percutaneous ultrasonication on intrathecally administered plasmid DNA and echo-contrast microbubbles enhanced the gene transfer into spinal meningeal cells in mice. The present approach can provide some advantages specific to spinal gene therapy including minimal invasiveness, regional targetability, and possible paracrine delivery of therapeutic molecules to the spinal nerve system. Studies including functional assessments of therapeutic gene transfer as well as the application of the techniques in larger animals will further clarify the feasibility of the present ultrasound–microbubble method in spinal gene therapy.

References

[1] J.C. Glorioso, D.J. Fink, Herpes vector-mediated gene transfer in treatment of diseases of the nervous system, Annu. Rev. Microbiol. 58 (1) (2004) 253–271.
[2] S.P. Wilson, Gene-based therapy for treatment of chronic pain, Semin. Pain Med. 1 (4) (2003) 220–226.
[3] F. Facchiano, E. Fernandez, S. Mancarella, G. Maira, M. Miscusi, D. D'Arcangelo, G. Cimino-Reale, M.L. Falchetti, M.C. Capogrossi, R. Pallini, Promotion of regeneration of corticospinal tract axons in rats with recombinant vascular endothelial growth factor alone and combined with adenovirus coding for this factor, J. Neurosurg. 97 (1) (2002) 161–168.
[4] M. Koda, M. Hashimoto, M. Murakami, K. Yoshinaga, O. Ikeda, M. Yamazaki, S. Koshizuka, T. Kamada, H. Moriya, H. Shirasawa, S. Sakao, H. Ino, Adenovirus vector-mediated in vivo gene transfer of brain-derived neurotrophic factor (BDNF) promotes rubrospinal axonal regeneration and functional recovery after complete transection of the adult rat spinal cord, J. Neurotrauma 21 (3) (2004) 329–337.
[5] X.Q. Tang, Y. Wang, Z.H. Huang, J.S. Han, Y. Wan, Adenovirus-mediated delivery of GDNF ameliorates corticospinal neuronal atrophy and motor function deficits in rats with spinal cord injury, NeuroReport 15 (3) (2004) 425–429.
[6] S.P. Wilson, D.C. Yeomans, M.A. Bender, Y. Lu, W.F. Goins, J.C. Glorioso, Antihyperalgesic effects of infection with a preproenkephalin-encoding herpes virus, Proc. Natl. Acad. Sci. U. S. A. 96 (6) (1999) 3211–3216.
[7] A.A. Finegold, A.J. Mannes, M.J. Iadarola, A paracrine paradigm for in vivo gene therapy in the central nervous system: treatment of chronic pain, Hum. Gene Ther. 10 (7) (1999) 1251–1257.
[8] M. Pohl, J. Braz, Gene therapy of pain: emerging strategies and future directions, Eur. J. Pharmacol. 429 (1–3) (2001) 39–48.
[9] M. Mata, J. Glorioso, D.J. Fink, Development of HSV-mediated gene transfer for the treatment of chronic pain, Exp. Neurol. 184 (Suppl. 1) (2003) S25–S29.
[10] P.A. Dijkmans, L.J.M. Juffermans, R.J.P. Musters, A. van Wamel, F.J. ten Cate, W. van Gilst, C.A. Visser, N. de Jong, O. Kamp, Microbubbles and ultrasound: from diagnosis to therapy, Eur. J. Echocardiog. 5 (4) (2004) 245–256.
[11] R. Bekeredjian, P.A. Grayburn, R.V. Shohet, Use of ultrasound contrast agents for gene or drug delivery in cardiovascular medicine, J. Am. Coll. Cardiol. 45 (3) (2005) 329–335.
[12] T. Kodama, Y. Tomita, K. Koshiyama, M.J.K. Blomley, Transfection effect of microbubbles on cells in superposed ultrasound waves and behavior of cavitation bubble, Ultrasound Med. Biol. 32 (6) (2006) 905–914.
[13] J.L. Hylden, G.L. Wilcox, Intrathecal morphine in mice: a new technique, Eur. J. Pharmacol. 67 (2–3) (1980) 313–316.
[14] B.W. Rice, M.D. Cable, M.B. Nelson, In vivo imaging of light-emitting probes, J. Biomed. Opt. 6 (4) (2001) 432–440.
[15] K.M. Hargreaves, R. Dubner, F. Brown, C. Flores, J. Joris, A new and sensitive method for measuring thermal nociception in cutaneous hyperalgesia, Pain 32 (1) (1988) 77–88.
[16] J.D. Hommel, R.M. Sears, D. Georgescu, D.L. Simmons, R.J. DiLeone, Local gene knockdown in the brain using viral-mediated RNA interference, Nat. Med. 9 (12) (2003) 1539–1544.
[17] C.R. Dass, P.F. Choong, Selective gene delivery for cancer therapy using cationic liposomes: in vivo proof of applicability, J. Control. Release 113 (2) (2006) 155–163.
[18] C.M. Newman, A. Lawrie, A.F. Brisken, D.C. Cumberland, Ultrasound gene therapy: on the road from concept to reality, Echocardiography 18 (4) (2001) 339–347.
[19] R. Bekeredjian, S. Chen, P.A. Frenkel, P.A. Grayburn, R.V. Shohet, Ultrasound-targeted microbubble destruction can repeatedly direct highly specific plasmid expression to the heart, Circulation 108 (8) (2003) 1022–1026.
[20] Y. Taniyama, K. Tachibana, K. Hiraoka, T. Namba, K. Yamasaki, N. Hashiya, M. Aoki, T. Ogihara, K. Yasufumi, R. Morishita, Local delivery of plasmid DNA into rat carotid artery using ultrasound, Circulation 105 (10) (2002) 1233–1239.
[21] Y. Taniyama, K. Tachibana, K. Hiraoka, M. Aoki, S. Yamamoto, K. Matsumoto, T. Nakamura, T. Ogihara, Y. Kaneda, R. Morishita, Development of safe and efficient novel nonviral gene transfer using ultrasound: enhancement of transfection efficiency of naked plasmid DNA in skeletal muscle, Gene Ther. 9 (6) (2002) 372–380.
[22] M. Shimamura, N. Sato, Y. Taniyama, M. Endo, H. Kurinami, M. Aoki, T. Ogihara, Y. Kaneda, R. Morishita, Development of efficient plasmid DNA transfer into adult rat central nervous system using microbubble-enhanced ultrasound, Gene Ther. 11 (20) (2004) 1532–1539.
[23] M. Shimamura, N. Sato, Y. Taniyama, H. Kurinami, H. Tanaka, T. Takami, M. Ogihara, Y. Tohyama, R. Morishita, Gene transfer into adult rat spinal cord using naked DNA and ultrasound microbubbles, J. Gene Med. 7 (11) (2005) 1468–1474.
[24] A. Aoi, K. Konno, S. Fumiaki, S. Mori, G. Vassaux, T. Kodama, HSV-tk/GCV cytotoxic gene therapy using ultrasound and nanobubbles, Ultrasound Med. Biol. 32 (5S) (2006) 280.
[25] C.R. Lin, M.H. Tai, J.T. Cheng, A.K. Chou, J.J. Wang, P.H. Tan, M. Marsala, L.C. Yang, Electroporation for direct spinal gene transfer in rats, Neurosci. Lett. 317 (1) (2002) 1–4.
[26] T.H. Lee, L.C. Yang, A.K. Chou, P.C. Wu, C.R. Lin, C.H. Wang, J.T. Chen, C.S. Tang, In vivo electroporation of proopiomelanocortin induces analgesia in a formalin-injection pain model in rats, Pain 104 (1–2) (2003) 159–167.
[27] J.R. Lindner, Microbubbles in medical imaging: current applications and future directions, Nat. Rev. Drug Discov. 3 (6) (2004) 527–532.

Journal of Drug Targeting, August–September 2007; 15(7–8): 507–517

informa
healthcare

Preclinical and clinical studies of anticancer drug-incorporated polymeric micelles

YASUHIRO MATSUMURA

Investigative Treatment Division, Research Center for Innovative Oncology, National Cancer Center Hospital East, Kashiwa, Chiba, Japan

Abstract
Tumour-targeted delivery of therapeutic agents is a longstanding pharmacological goal to improve selectivity and Therapeutic Index. Most scientists have sought to use 'active' receptor-mediated tumour-targeting systems, however the 'passive' targeting afforded by the Enhanced Permeability and Retention (EPR) effects provides a versatile and non-saturable opportunity for tumour-selective delivery. Polymeric micelles are ideally suited to exploit the EPR effect, and they have been used for the delivery of a range of anticancer drugs in preclinical and clinical studies. Here I overview some of the more important approaches, assessing usefulness and seeking to identify the most promising ways to apply the phenomenon of passive targeting for improved clinical outcome.

Keywords: *Micelles, anticancer agent, EPR effect, clinical trial*

Preface

Several problems of anticancer agents are recognized, such as their low therapeutic indices and limited efficacy due to the nonselective nature of their therapeutic targets and their inability to accumulate selectively in cancer tissues. Therefore, it would be desirable to develop modalities by which cytotoxic drugs can be selectively targeted to tumour tissues and allowed to act effectively on only the cancer cells in the tumor. The role of drug delivery systems (DDS) has drawn attention in this context. DDS could be used for active or passive targeting of tumor tissues. The former refers to the development of monoclonal antibodies directed against tumour-related molecules that allow targeting of the tumour, because of specific binding between the antibody and its antigen. However, the application of DDS using monoclonal antibodies is restricted to tumours expressing high levels of related antigens.

About a quarter of a century ago, after training as a surgeon, I started my career in the field of DDS under the supervision of Prof. Maeda. We made intensive efforts to ascertain the mechanism of accumulation of macromolecules in solid tumours. Finally, we succeeded in publishing the first paper, in 1986, on the enhanced permeability and retention (EPR) effect (Matsumura and Maeda 1986). Passive targeting is based on this EPR effect. The EPR effect is based on the pathophysiological characteristics of solid tumour tissues: hypervascularity, incomplete vascular architecture, secretion of vascular permeability factors stimulating extravasation within cancer tissue, and absence of effective lymphatic drainage from tumours that impedes the efficient clearance of macromolecules accumulated in solid tumour tissues.

Several techniques to maximally use the EPR effect have been developed, e.g. modification of drug structures and development of drug carriers. Polymeric micelle-based anticancer drugs were originally developed by Prof. Kataoka et al. in late the 1980's or early 1990's (Yokoyama et al. 1990; 1991a, b, c; Kataoka et al. 1993). Polymeric micelles were expected to increase the accumulation of drugs in tumour tissues utilizing the EPR effect and to incorporate various kinds of drugs into the inner core by chemical conjugation or physical entrapment with relatively high stability. The size of the micelles

Correspondence: Y. Matsumura, Investigative Treatment Division, Research Center for Innovative Oncology, National Cancer Center Hospital East, Kashiwa, Chiba, Japan.

ISSN 1061-186X print/ISSN 1029-2330 online
DOI: 10.1080/10611860701499888

can be controlled within the diameter range of 20–100 nm, to ensure that the micelles do not pass through normal vessel walls; therefore, a reduced incidence of the side effects of the drugs may be expected due to the decreased volume of distribution.

In this chapter, polymeric micelle systems for which clinical trials are now underway are reviewed.

NK105, paclitaxel-incorporating micellar nanoparticle

Paclitaxel (PTX) is one of the most useful anticancer agents known for various cancers, including ovarian, breast and lung cancers (Carney 1996; Khayat et al. 2000). However, PTX has serious adverse effects, e.g. neutropenia and peripheral sensory neuropathy. In addition, anaphylaxis and other severe hypersensitive reactions have been reported to develop in 2–4% of patients receiving the drug even after premedication with antiallergic agents; these adverse reactions have been attributed to the mixture of Cremophor EL and ethanol which was used to solubilize PTX (Weiss et al. 1990; Rowinsky and Donehower 2003). Of the adverse reactions, neutropenia can be prevented or managed effectively by administering a granulocyte colony-stimulating factor. On the other hand, there are no effective therapies to prevent or reduce nerve damage which is associated with peripheral neuropathy caused by PTX; therefore, neurotoxicity constitutes a significant dose-limiting toxicity (DLT) of the drug (Rowinsky et al. 1993; Wasserheit et al. 1996).

Preparation and characterization of NK105

To construct NK105 micellar nanoparticles (Figure 1), block copolymers consisting of polyethylene glycol (PEG) and polyaspartate, so-called PEG-polyaspartate described previously (Yokoyama et al. 1990; 1991a, b, c; Kataoka et al. 1993), were used. PTX was incorporated into polymeric micelles formed by physical entrapment utilizing hydrophobic interactions between PTX and the block copolymer polyaspartate chain. After screening of many candidate substances, 4-phenyl-1-butanol was employed for the chemical modification of the polyaspartate block to increase its hydrophobicity. Treating with a condensing agent, 1,3-diisopropylcarbodiimide, the half of carboxyl groups on the polyaspartate were esterified with 4-phenyl-1-butanol. Molecular weight of the polymers was determined to be approximately 20,000, (PEG block: 12,000; modified polyaspartate block: 8000). NK105 was prepared by facilitating the self-association of NK105 polymers and PTX. NK105 was obtained as a freeze-dried formulation and contained *ca.* 23% (w/w) of PTX, as determined by reversed-phase liquid-chromatography using an ODS column with mobile phase consisting of acetonitrile and water (9:11, v/v) and detection of ultraviolet absorbance at 227 nm. Finally, NK105, a PTX-incorporating polymeric micellar nanoparticle formulation with a single and narrow size distribution, was obtained. The weight-average diameter of the nanoparticles was approximately 85 nm ranging from 20 to 430 nm.

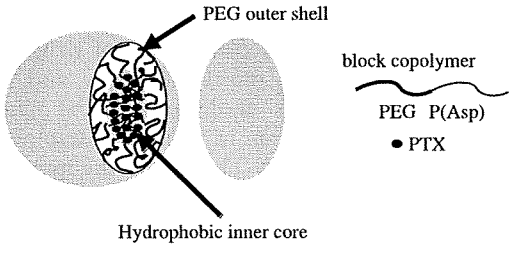

Figure 1. Preparation and characterization of NK105. The micellar structure of NK105 PTX was incorporated into the inner core of the micelle.

Pharmacokinetics and pharmacodynamics of NK105

Colon 26-bearing CDF1 mice were given a single iv injection of PTX 50 or 100 mg/kg, or of NK105 at an equivalent dose of PTX. Subsequently, the time-course changes in the plasma and tumour levels of PTX were determined in the PTX and NK105 administration groups; furthermore, the pharmacokinetic parameters of each group were also determined. NK105 exhibited slower clearance from the plasma than PTX, while NK105 was present in the plasma for up to 72 h after injection; PTX was not detected after 24 h or later of injection. The plasma concentration at 5 min ($C_{5\,min}$) and the AUC of NK105 were 11- to 20-fold and 50- to 86-fold higher for NK105 than for PTX, respectively. Furthermore, the half-life at the terminal phase ($t_{1/2}z$) was 4–6 times longer for NK105 than for PTX. The maximum concentration (C_{max}) and AUC of NK105 in Colon 26 tumours were approximately 3 times and 25 times higher for NK105 than for PTX, respectively. NK105 continued to accumulate in the tumours until 72 h after injection. The tumour PTX concentration was higher than 10 μg/g even at 72 h after the intravenous injection of NK105 50 and 100 mg/kg. By contraries, the tumour PTX concentrations at 72 h after the intravenous administration of free PTX 50 and 100 mg/kg were below detection limits and less than 0.1 μg/g, respectively.

In vivo *antitumour activity*

BALB/c mice bearing s.c. HT-29 colon cancer tumours showed decreased tumour growth rates after the administration of PTX and NK105. However, NK105 exhibited superior antitumour activity as compared with PTX ($P < 0.001$). The

antitumour activity of NK105 administered at a PTX-equivalent dose of 25 mg/kg was comparable to that obtained after the administration of free PTX 100 mg/kg. Tumour suppression by NK105 increased in a dose-dependent manner. Tumours disappeared after the first dosing to mice treated with NK105 at a PTX-equivalent dose of 100 mg/kg, and all mice remained tumour-free thereafter. In addition, less weight loss was induced in mice which were given NK105 100 mg/kg than in those which were given the same dose of free PTX.

Neurotoxicity of PTX and NK105

Treatment with PTX has resulted in cumulative sensory-dominant peripheral neurotoxicity in humans, characterized clinically by numbness and/or paraesthesia of the extremities. Pathologically, axonal swelling, vesicular degeneration, and demyelination were observed. We, therefore, examined the effects of free PTX and NK105 using both electrophysiological and morphological methods.

Prior to drug administration, there were no significant differences in the amplitude of caudal sensory nerve action potential (caudal SNAP) between two drug administration groups. On day 6 after the last dosing (at week 6), the amplitude of the caudal SNAP in the control group increased in association with rat maturation. The amplitude was significantly smaller in the PTX group than in the control group ($P < 0.01$), while the amplitude was significantly larger in the NK105 group than in the PTX group ($P < 0.05$) and was comparable between the NK105 group and the control group (Figure 2). Histopathological examination of longitudinal paraffin-embedded sections of the sciatic nerve 5 days after the sixth weekly injection revealed degenerative changes. The NK105 administration group showed only a few degenerative myelinated fibers in contrast to the PTX administration group which indicated markedly more numerous degenerative myelinated fibers.

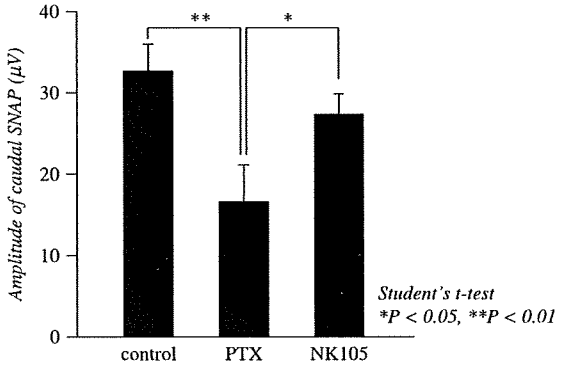

Figure 2. Effects of PTX or NK105 on the amplitude of rat caudal sensory nerve action potentials as examined 5 days after weekly injections for 6 weeks. Rats ($n = 14$) were injected with NK105 or PTX at a PTX-equivalent dose of 7.5 mg/kg. About 5% glucose was also injected in the same manner to animals in the control group.

Clinical study

A phase I study was designed to determine maximum tolerated dose (MTD), DLTs, the recommended dose (RD) for phase II and the pharmacokinetics of NK105 (Kato et al.).

NK105 was administered by 1-hour intravenous infusion every 3 weeks without anti-allergic premedication. The starting dose was 10 mg PTX equivalent/m^2, and dose escalated according to the accelerated titration method. To date, 17 patients (pts) have been treated at the following doses: 10 mg/m^2 ($n = 1$); 20 mg/m^2 ($n = 1$); 40 mg/m^2 ($n = 1$); 80 mg/m^2 ($n = 1$); 110 mg/m^2 ($n = 3$); 150 mg/m^2 ($n = 5$); 180 mg/m^2 ($n = 5$). Tumor types treated have included: pancreatic ($n = 9$), bile duct ($n = 5$), gastric ($n = 2$), and colon ($n = 1$). Neutropenia has been the predominant hematological toxicity and grade 3 or 4 neutropenia was observed in pts treated at 110, 150 and 180 mg/m^2. One patient at 180 mg/m^2 developed grade 3 fever. No other grade 3 or 4 non-hematological toxicity including neuropathies was observed. DLTs were observed in pts with at the 180 mg/m^2 (grade 4 neutropenia lasting for more than 5 days), which was determined as MTD. Allergic reactions were not observed in any of the patients except one patient at the 180 mg/m^2. A partial response was observed in one pancreatic cancer pt who received more than 12 courses of NK105 (Figure 3). Despite of the long time usage, only grade 1 or 2 neuropathy was observed by modifying the dose or period of drug administration. Colon and gastric cancer pts experienced stable disease lasting 10 and 7 courses, respectively. The C_{max} and AUC of NK105 showed dose-dependent characteristics. The plasma AUC of NK105 at 180 mg/m^2 was approximately 30-fold higher than that of commonly-used paclitaxel formulation.

Accrual is ongoing at the 150 mg/m^2 dose level to determine RD. DLT was grade 4 neutropenia. NK105 generates prolonged systemic exposure to PTX in plasma. Tri-weekly 1-hour infusion of NK105 was feasible and well tolerated, with antitumor activity in pancreatic cancer pt. NK105 is planning to be evaluated in Phase II studies of patients with pancreatic, gastric, or ovarian cancer.

NC-6004, cisplatin-incorporating micellar nanoparticle

Cisplatin [*cis*-dichlorodiammineplatinum (II): CDDP] is a key drug in the chemotherapy for cancers, including lung, gastrointestinal, and genitourinary cancer (Roth 1996; Horwich et al. 1997). However, we often find that it is necessary to

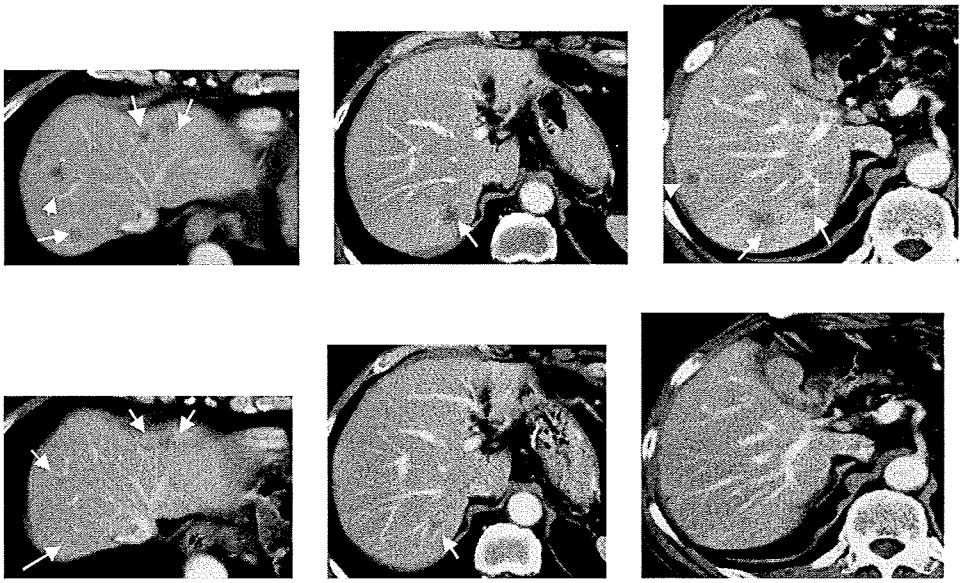

Figure 3. Serial CT scans. (A) A 60-year-old male with pancreatic cancer who was treated with NK105 at a dose level of 150 mg/m^2. Baseline scan (upper panels) showing multiple metastasis in the liver. Partial response, characterized by a more than 90% decrease in the size of the liver metastasis (lower panels) compared with the baseline scan. The antitumor response was maintained for nearly 1 year.

discontinue treatment with CDDP due to its adverse reactions, e.g. nephrotoxicity and neurotoxicity, despite its persisting effects (Pinzani et al. 1994). Platinum analogues, e.g. carboplatin and oxaliplatin (Cleare et al. 1978), have been developed to date to overcome these CDDP-related disadvantages. Consequently, these analogues are becoming the standard drugs for ovarian cancer (du Bois et al. 2003) and colon cancer (Cassidy et al. 2004). However, those regimens including CDDP are considered to constitute the standard treatment for lung cancer, stomach cancer, testicular cancer (Horwich et al. 1997), and urothelial cancer (Bellmunt et al. 1997). Therefore, the development of a DDS technology is anticipated, which would offer the better selective accumulation of CDDP into solid tumours while lessening its distribution into normal tissue.

Preparation and characterization of NC-6004

NC-6004 were prepared according to the slightly modified procedure reported by Nishiyama et al. (2003) (Figure 4). NC-6004 consists of PEG, a hydrophilic chain which constitutes the outer shell of the micelles, and the coordinate complex of poly(glutamic acid) (P(Glu)) and CDDP, a polymer-metal complex-forming chain which constitutes the inner core of the micelles. The molecular weight of PEG-P(Glu) as a sodium salt was approximately 18,000 (PEG: 12,000; P(Glu): 6000). The CDDP-incorporated polymeric micelles were clearly discriminated from typical micelles from amphiphilic block copolymers. The driving force of the formation of the CDDP-incorporated micelles is the ligand substitution of platinum(II) atom from chloride to carboxylate in the side chain of P(Glu). The molar ratio of CDDP to the carboxyl groups in the copolymers was 0.71 (Nishiyama et al. 2003). A narrowly distributed size of polymeric micelles (30 nm) was confirmed by the dynamic light scattering (DLS) measurement. Also, the static light scattering (SLS) measurement revealed that the CDDP-loaded micelles showed no dissociation upon dilution and the CMC was less than 5×10^{-7}, suggesting remarkable stability compared with typical micelles from amphiphilic block copolymers (Nishiyama et al. 2003). It is assumed that the interpolymer cross-linking by Pt(II) atom might contribute to stabilization of the micellar structure.

The release rates of CDDP from NC-6004 were 19.6 and 47.8% at 24 and 96 h, respectively. In distilled water, furthermore, NC-6004 was stable without releasing cisplatin.

Pharmacokinetics and pharmacodynamics

FAAS could measure serum concentrations of platinum up to 48 h after i.v. injection of NC-6004 but could measure them only up to 4 h after i.v. injection of CDDP. NC-6004 showed a very long blood retention profile as compared with CDDP. The AUC_{0-t} and C_{max} values were significantly higher in animals given NC-6004 than in animals given CDDP, namely, 65-fold and 8-fold, respectively, ($P < 0.001$ and 0.001, respectively). Furthermore, the CL_{tot} and Vss values were significantly lower in animals given NC-6004 than in animals given

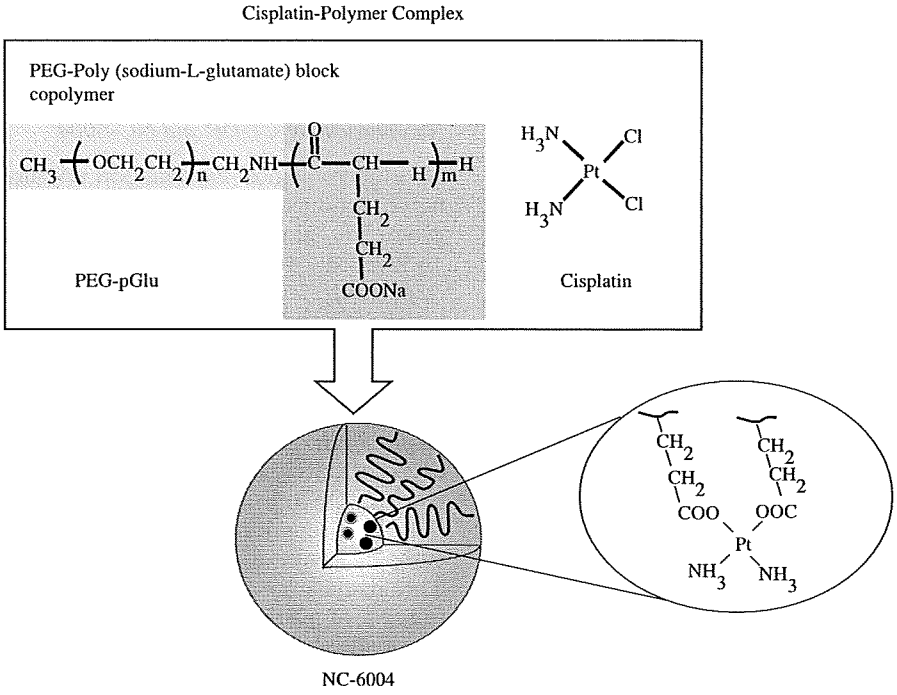

Figure 4. Preparation and characterization of cisplatin-incorporating polymeric micelles (NC-6004). Chemical structures of cisplatin (CDDP) and polyethylene glycol poly(glutamic acid) block copolymers [PEG-P(Glu) block copolymers], and the micellar structures of CDDP-incorporating polymeric micelles (NC-6004).

CDDP, i.e. one-nineteenth and one-seventy fifth, respectively, ($P < 0.01$ and 0.01, respectively).

Regarding the concentration–time profile of platinum in various tissues after i.v. injection of CDDP or NC-6004, all organs measured exhibited the highest concentrations of platinum within 1 h after administration in all animals given CDDP. Furthermore, animals given NC-6004 exhibited the highest tissue concentrations of platinum in the liver and spleen at late time points (24 and 48 h after administration, respectively). However, the concentrations decreased on day 7 after administration. In addition, and in a similar manner to other drugs, which are incorporated in polymeric carriers, NC-6004 demonstrated accumulation in organs of the reticuloendothelial system, e.g. liver and spleen. At 48 h after administration, tissue concentrations of platinum in the liver and spleen were 4.6- and 24.4-fold higher for NC-6004 than for CDDP. On the other hand, a marked increase in tissue platinum concentration was observed immediately after administration in the kidneys of animals given CDDP. Renal platinum concentration at 10 min and 1 h after administration were 11.6- and 3.1-fold lower, respectively, in animals given NC-6004 than in animals given CDDP. Furthermore, the maximum concentration (C_{max}) in the kidney was 3.8-fold lower at the time of NC-6004 administration than at the time of CDDP administration.

Regarding the tumour accumulation of platinum, tumour concentrations of platinum peaked at 10 min after administration of CDDP. On the other hand, tumour concentrations of platinum peaked at 48 h after administration of NC-6004. The maximum concentration (C_{max}) in tumour was 2.5-fold higher for NC-6004 than for CDDP ($P < 0.001$). Furthermore, the tumour AUC was 3.6-fold higher for NC-6004 than for CDDP (81.2 and 22.6 μg/ml h in animals given NC-6004 and CDDP, respectively).

In vivo *antitumour activity*

BALB/c nude mice implanted with a human gastric cancer cell line MKN-45 showed decreased tumour growth rates after i.v. injection of CDDP and NC-6004. In the administration of CDDP, the CDDP 5 mg/kg administration group showed a significant decrease ($P < 0.01$) in tumour growth rate as compared with the control group. However, the NC-6004 administration groups at the same dose levels as CDDP showed no significant difference in tumour growth rate. Regarding time-course changes in body weight change rate, the CDDP 5 mg/kg administration group showed a significant decrease ($P < 0.001$) in body weight as compared with the control group. On the other hand, NC-6004 administration group did not show a decrease in body weight as compared with the control group.

Nephrotoxicity of CDDP and NC-6004

In the CDDP 10 mg/kg administration group, 4 of 12 rats died from toxicity within 7 days after drug administration. No deaths occurred in the NC-6004 10 mg/kg administration group. Regarding renal function, the BUN concentrations on day 7 after the administration of 5% glucose, CDDP 10 mg/kg, and NC-6004 10 mg/kg were 20.8 ± 3.0, 65.3 ± 44.4 and 20 ± 4.5 mg/dl, respectively. The plasma concentrations of creatinine on day 7 after the administration of 5% glucose, CDDP 10 mg/kg, and NC-6004 10 mg/kg were 0.27 ± 0.03, 0.68 ± 0.23 and 0.28 ± 0.04 mg/dl, respectively. The CDDP 10 mg/kg administration group showed significantly higher plasma concentrations of BUN and creatinine as compared with the control group ($P < 0.05$ and 0.001, respectively), with the NC-6004 10 mg/kg administration group ($P < 0.05$ and 0.001, respectively) (Figure 5). Light microscopy indicated tubular dilation with flattening of the lining cells of the tubular epithelium in the kidney from all animals in the CDDP 10 mg/kg administration group. On the other hand, no histopathological change was observed in the kidneys from all animals in the NC-6004 10 mg/kg administration group.

Neurotoxicity of CDDP and NC-6004

Neurophysiological examination revealed that motor nerve conduction velocities (MNCVs) in animals given 5% glucose, CDDP, and NC-6004 were 44.2 ± 3.5, 40.94 ± 5.08 and 40.62 ± 0.63 m/s, respectively. No significant difference was found among the groups with respect to MNCV. Furthermore, sensory nerve conduction velocities (SNCVs) in animals given 5% glucose, CDDP, and NC-6004 were 42.86 ± 8.07, 35.48 ± 4.91 and 43.74 ± 5.3 m/s, respectively. Animals given NC-6004 showed no delay in SNCV as compared with animals given 5% glucose. On the other hand, animals given CDDP showed a significant delay ($P < 0.05$) in SNCV as compared with animals given NC-6004 (Figure 6). The analysis by ICP-MS on sciatic nerve concentrations of platinum could not detect platinum in the sciatic nerve from animals given 5% glucose (data not shown). Sciatic nerve concentrations of platinum

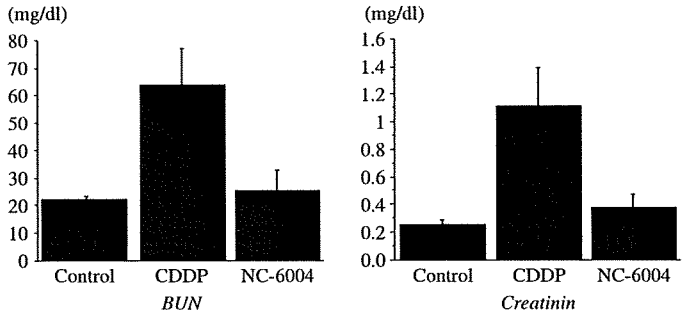

Figure 5. Nephrotoxicity of CDDP and NC-6004. Plasma concentrations of blood urea nitrogen (BUN) and creatinine were measured after a single i.v. injection of 5% glucose ($n = 8$), CDDP at a dose of 10 mg/kg ($n = 12$), NC-6004 at a dose of 10 mg/kg ($n = 13$) on a CDDP basis.

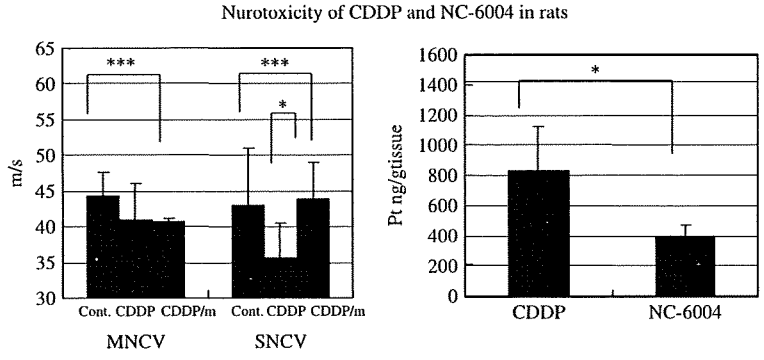

Figure 6. Neurotoxicity of CDDP and NC-6004 in rats. Rats ($n = 5$) were given CDDP (2 mg/kg), NC-6004 (an equivalent dose of 2 mg/kg CDDP), or 5% glucose, all intravenously twice a week, 11 administrations in total. Sensory nerve conduction velocity (SNCV) and motor nerve conduction velocity (MNCV) of the sciatic nerve at week 6 after the initial administration. The platinum concentration in the sciatic nerve. Rats were given CDDP (5 mg/kg, $n = 5$), NC-6004 (an equivalent dose of 5 mg/kg CDDP, $n = 5$), or 5% glucose ($n = 2$), all intravenously twice a week, four administrations in total. On day 3 after the final administration, a segment of the sciatic nerve was removed and the platinum concentration in the sciatic nerve was measured by ICP-MS. The data are expressed as the mean ± SD $*P < 0.05$.

in animals given CDDP and NC-6004 were 827.2 ± 291.3 and 395.5 ± 73.1 ng/g tissue. Therefore, the concentrations were significantly ($P < 0.05$) lower in animals given NC-6004. This finding is believed to be a factor which reduced neurotoxicity following NC-6004 administration as compared with the CDDP administration.

Present situation of a clinical study of NC-6004

A phase 1 clinical trial of NC-6004 is now under way in United Kingdom. Starting dose of NC-6004 was 10 mg/m^2. NC-6004 was administered once every 3 weeks with only 1000 ml water loading. In Japan, a phase 1 trial will be stared soon in the National Cancer Center Hospital.

NK012, SN-38-incorporating micellar nanoparticle

The antitumor plant alkaloid camptothecin (CPT) is a broad-spectrum anticancer agent which targets the DNA topoisomerase I. Although CPT has showed promising antitumor activity *in vitro* and *in vivo* (Gallo et al. 1971; Li et al. 1972), it has not been used clinically because of its low therapeutic efficacy and severe toxicity (Gottlieb et al. 1970; Muggia et al. 1972). Among CPT analogs, irinotecan hydrochloride (CPT-11) has recently been demonstrated to be active against colorectal, lung, and ovarian cancer (Cunningham et al. 1998; Saltz et al. 2000; Noda et al. 2002, Negoro et al. 2003; Bodurka et al. 2003). CPT-11 itself is a prodrug and is converted to 7-ethyl-10-hydroxy-CPT (SN-38), a biologically active metabolite of CPT-11, by carboxylesterases (CEs). SN-38 exhibits up to 1000-fold more potent cytotoxic activity against various cancer cells *in vitro* than CPT-11 (Takimoto and Arbuck 2001). Although CPT-11 is converted to SN-38 in the liver and tumor, the metabolic conversion rate is less than 10% of the original volume of CPT-11 (Rothenberg et al. 1993; Slatter et al. 2000). In addition, the conversion of CPT-11 to SN-38 depends on the genetic inter-individual variability of CE activity (Guichard et al. 1999). Thus, direct use of SN-38 might be of great advantage and attractive for cancer treatment. For the clinical use of SN-38, however, it is essential to develop a soluble form of water-insoluble SN-38. The progress of the manufacturing technology of "micellar nanoparticles" may make it possible to use SN-38 for *in vivo* experiments and further clinical use.

Preparation and characterization of NK012

NK012 is an SN-38-loaded polymeric micelle constructed in an aqueous milieu by the self-assembly of an amphiphilic block copolymers, PEG-PGlu(SN-38). The molecular weight of PEG-PGlu(SN-38) was determined to be approximately 19,000 (PEG segment: 12,000; SN-38-conjugated PGlu segment: 7000). NK012 was obtained as a freeze-dried formulation and contained *ca.* 20% (w/w) of SN-38 (Figure 7). The mean particle size of NK012 is 20 nm in diameter with a relatively narrow range. The releasing rates of SN-38 from NK012 in phosphate buffered saline at 37°C were 57 and 74% at 24 and 48 h, respectively, and that in 5% glucose solution at 37°C were 1 and 3% at 24 and 48 h, respectively. These results indicate that NK012 can release SN-38 under neutral condition even without the presence of a hydrolytic enzyme, and is stable in 5% glucose solution. It is suggested that NK012 is stable before administration and starts to release SN-38, the active component, under physiological conditions after administration.

Cellular sensitivity of NSCLC and colon cancer cells to SN-38, NK012, and CPT-11

The IC_{50} values of NK012 for the cell lines ranged from 0.009 μM (Lovo cells) to 0.16 μM (WiDR cells). The growth-inhibitory effects of NK012 are 43–340 fold more potent than those of CPT-11, whereas the IC_{50} values of NK012 were 2.3–5.8 fold higher than those of SN-38.NK012 exhibited a higher cytotoxic effect against each cell line as compared with CPT-11 (× 43–340 fold sensitivity). On the other hand, the IC_{50} values of NK012 were a little higher than those of SN-38, similar to the cytotoxic feature also reported in a previous study about micellar drugs (Uchino et al. 2005).

Pharmacokinetic analysis of NK012 and CPT-11 using HT-29-bearing nude mice

After injection of CPT-11, the concentrations of CPT-11 and SN-38 for plasma declined rapidly with time in a log-linear fashion. On the other hand, NK012 (polymer-bound SN-38) exhibited slower clearance. The clearance of NK012 in the HT-29 tumor was significantly slower and the concentration of free SN-38 was maintained at more than 30 ng/g even at 168 h after injection.

Anti-tumor activity and the distribution of NK012 and CPT-11 in SBC-3/Neo or SBC-3/VEGF tumors

In order to determine whether the potent antitumor effect of NK012 is enhanced in the tumors with high vascularity, we used vascular endothelial growth factor-secreting cells SBC-3/VEGF. There was no significant difference in the *in vitro* cytotoxic activity of each drug between SBC-3/Neo and SBC-3/VEGF. Gross findings of SBC-3/VEGF tumors are reddish as compared with SBC-3/Neo tumors. Deviating from the ordinary experimental tumor model, tumors were allowed to

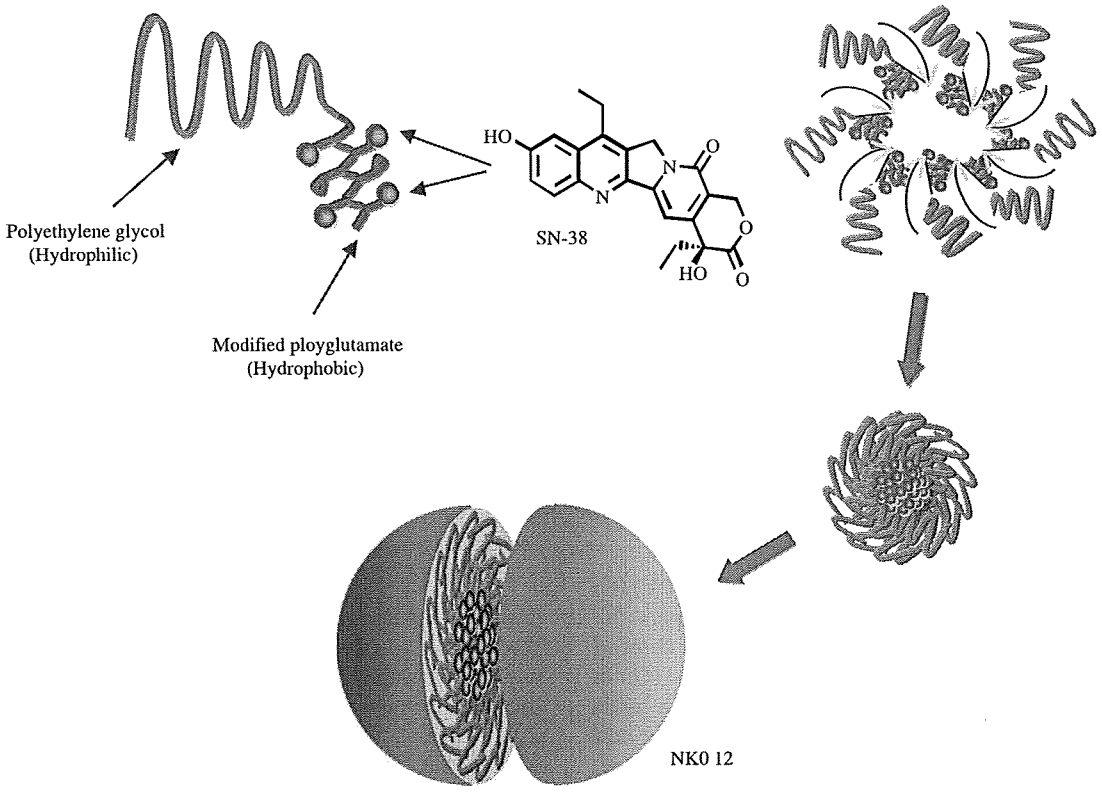

Figure 7. Schematic structure of NK012. A polymeric micelle carrier of NK012 consists of a block copolymer of PEG (molecular weight of about 5000) and partially modified polyglutamate (about 20 unit). Polyethylene glycol (hydrophilic) is believed to be the outer shell and SN-38 was incorporated into the inner core of the micelle.

grow until they became massive in size, around 1.5 cm (Figure 8), and then the treatment was initiated. NK012 at doses of 15 and 30 mg/kg showed potent anti-tumor activity against bulky SBC-3/Neo tumors (1533.1 ± 1204.7 mm^3) as compared with CPT-11 (Figure 8). Striking antitumor activity was observed in mice treated with NK012 (Figure 8) when we compared the antitumor activity of NK012 with CPT-11 using SBC-3/VEGF cells. SBC-3/VEGF bulky masses (1620.7 ± 834.0 mm^3) disappeared in all mice, although relapse 3 months after treatment was noted in one mouse treated with NK012 20 mg/kg (Figure 8). On the other hand,

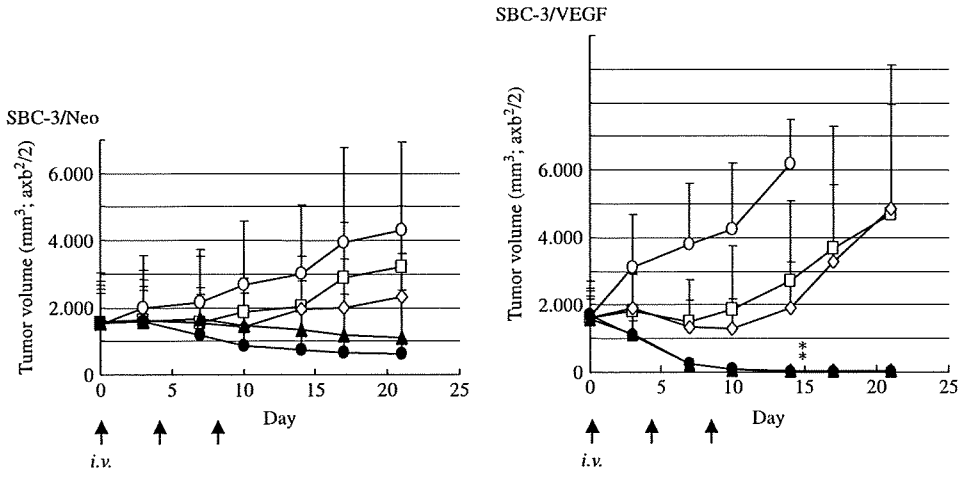

Figure 8. Intravenous administration of NK012 or CPT-11 was started when the mean tumor volumes of groups reached a massive 1500 mm^3. The mice were divided into test group (□: control; □: CPT-11 20 mg/kg/day; □: CPT-11 40 mg/kg/day; ▲: NK012 15 mg/kg/day; and □: NK012 30 mg/kg/day). NK012 or CPT-11 was administered i.v. on days 0, 4 and 8. Each group consisted of 4 mice. $*P < 0.05$.

SBC-3/VEGF were not eradicated and rapidly regrew after a partial response in mice treated with CPT-11. Approximate 10% body weight loss was observed in mice treated with NK012 20 mg/kg, but no significant difference was observed in comparison with mice treated with CPT-11 30 mg/kg.

We then examined the distribution of free SN-38 in the SBC-3/Neo and SBC-3/VEGF masses after administration of NK012 and CPT-11. In the case of CPT-11 administration, the concentrations at 1 and 6 h after the administration were less than 100 ng/g both in the SBC-3/Neo and SBC-3/VEGF tumors, and were almost negligible at 24 h in both tumors. There was no significant difference in the concentration between the SBC-3/Neo and SBC-3/VEGF tumors. On the other hand, in the case of NK012 administration, free SN-38 was detectable in the tumors even at 72 h after the administration. The concentrations of free SN-38 were higher in the SBC-3/VEGF tumors than those in the SBC-3/Neo tumors at any time point during the period of observation (significant at 1, 6, 24 h. $*P < 0.05$).

Tissue distribution of SN-38 after administration of NK012 and CPT-11

We examined the concentration–time profile of free SN-38 in various tissues after i.v. administration of NK012 and CPT-11. All organs measured exhibited the highest concentration of SN-38 at 1 h after administration in mice given CPT-11. On the other hand, mice given NK012 exhibited prolonged distribution in the liver and spleen. In a similar manner to other micellar drugs (Yokoyama et al. 1991a, b, c; Uchino et al. 2005), NK012 demonstrated relatively higher accumulation in organs of the reticuloendothelial system. In the lung, kidney and small intestine, the highest concentration of free SN-38 was achieved at 1 h after injection of NK012 and the concentration was almost negligible at 24 h. Although the concentrations of free SN-38 in the small intestine were relatively high at 1 h after administration of NK012 and CPT-11, those rapidly decreased. Interestingly, there was no significant difference in the kinetic character of free SN-38 in the small intestine between mice treated with NK012 and CPT-11.

Synergistic antitumour activity of the NK012 combined with 5-fluorouracil

In two phase III trials, the addition of CPT-11 to bolus or infusional 5FU/LV regimens clearly yielded greater efficacy than treatment with 5FU/LV alone, with a doubling of the tumor response rate and prolongation of the median survival time by 2–3 months (Douillard et al. 2000; Saltz et al. 2001).

We demonstrated that the novel SN-38-incorporating polymeric micelles, NK012, exerted superior antitumor activity and less toxicity as compared to CPT-11 (Koizumi et al. 2006). Therefore, we speculated that the use of NK012 in place of CPT-11 in combination with 5FU may also yield superior results.

Comparison of the antitumor effect of combined NK012/5FU and CPT-11/5FU. The therapeutic effect of CPT-11/5FU was apparently inferior to that of NK012/5FU or even NK012 alone at the MTD. A more potent antitumor effect, namely 100% CR rate, was obtained in the NK012 alone and NK012/5FU groups, as compared with the 0% CR rate in the CPT-11/5FU (Nakajima and Matsumura 2007).

Specificity of cell cycle perturbation. We studied the difference in the effects between NK012 and CPT-11 on the cell cycle. The data indicate that both NK012 and CPT-11 had a tendency to accumulate the cells in the S phase, although the effect of NK012 was stronger and maintained for a more prolonged period than that of CPT-11. The histograms show aneuploidy of the tumor and that administration of NK012 or CPT-11 caused apoptosis of a proportion of the tumor cells (Nakajima and Matsumura 2007).

Present situation of a clinical study of NK012

A phase 1 study of NK012 is now under way in the National Cancer Center, Tokyo and Kashiwa in patients with advanced solid tumours. NK012 is infused intravenously over 60 min every 21 days until disease progression or unacceptable toxicity occurs.

Conclusion

A quarter of a century has passed since the EPR effect was discovered (Matsumura and Maeda 1986). Now the phrase EPR has become a fundamental principle in the field of DDS. Until recently, the EPR had not been recognized in the field of oncology. However, many oncologists have now become acquainted with it, since some drugs such as doxil, abraxane, and several PEGylated proteinacious agents formulated based on the EPR have been approved in the field of oncology. Micelle carrier systems described in this chapter are obviously categorized as DDS based on the EPR. I believe that some anticancer agents incorporating micelle nanoparticles may be approved for clinical use soon.

Our next task is to develop DDS utilizing the EPR effect, which can accumulate selectively in solid tumours but also allow distribution of the delivered

bullets (anticancer agents) through the entire mass of the solid tumor tissue.

References

Bellmunt J, Ribas A, Eres N, Albanell J, Almanza C, Bermejo B, Sole LA, Baselga J. 1997. Carboplatin-based versus cisplatin-based chemotherapy in the treatment of surgically incurable advanced bladder carcinoma. Cancer 80:1966–1972.

Bodurka DC, Levenback C, Wolf JK, Gano J, Wharton JT, Kavanagh JJ, et al. 2003. Phase II trial of irinotecan in patients with metastatic epithelial ovarian cancer or peritoneal cancer. J Clin Oncol 21:291–297.

Carney DN. 1996. Chemotherapy in the management of patients with inoperable non-small cell lung cancer. Semin Oncol 23:71–75.

Cassidy J, Tabernero J, Twelves C, Brunet R, Butts C, Conroy T, Debraud F, Figer A, Grossmann J, Sawada N, Schoffski P, Sobrero A, Van Cutsem E, Diaz-Rubio E. 2004. XELOX (capecitabine plus oxaliplatin): Active first-line therapy for patients with metastatic colorectal cancer. J Clin Oncol 22: 2084–2091.

Cleare MJ, Hydes PC, Malerbi BW, Watkins DM. 1978. Anti-tumor platinum complexes: Relationships between chemical properties and activity. Biochimie 60:835–850.

Cunningham D, Pyrhonen S, James RD, Punt CJ, Hickish TF, Heikkila R, et al. 1998. Randomised trial of irinotecan plus supportive care versus supportive care alone after fluorouracil failure for patients with metastatic colorectal cancer. Lancet 352: 1413–1418.

Douillard JY, Cunningham D, Roth AD, et al. 2000. Irinotecan combined with fluorouracil compared with fluorouracil alone as first-line treatment for metastatic colorectal cancer: A multicentre randomised trial. Lancet 355:1041–1047.

du Bois A, Luck HJ, Meier W, Adams HP, Mobus V, Costa S, Bauknecht T, Richter B, Warm M, Schroder W, Olbricht S, Nitz U, Jackisch C, Emons G, Wagner U, Kuhn W, Pfisterer J. 2003. A randomized clinical trial of cisplatin/paclitaxel versus carboplatin/paclitaxel as first-line treatment of ovarian cancer. J Natl Cancer Inst 95:1320–1329.

Gallo RC, Whang-Peng J, Adamson RH. 1971. Studies on the antitumor activity, mechanism of action, and cell cycle effects of camptothecin. J Natl Cancer Inst 46:789–795.

Gottlieb JA, Guarino AM, Call JB, Oliverio VT, Block JB. 1970. Preliminary pharmacologic and clinical evaluation of camptothecin sodium (NSC-100880). Cancer Chemother Rep 54: 461–470.

Guichard S, Terret C, Hennebelle I, Lochon I, Chevreau P, Fretigny E, et al. 1999. CPT-11 converting carboxylesterase and topoisomerase activities in tumour and normal colon and liver tissues. Br J Cancer 80:364–370.

Horwich A, Sleijfer DT, Fossa SD, Kaye SB, Oliver RT, Cullen MH, Mead GM, de Wit R, de Mulder PH, Dearnaley DP, Cook PA, Sylvester RJ, Stenning SP. 1997. Randomized trial of bleomycin, etoposide, and cisplatin compared with bleomycin, etoposide, and carboplatin in good-prognosis metastatic nonseminomatous germ cell cancer: A Multiinstitutional Medical Research Council/European Organization for Research and Treatment of Cancer Trial. J Clin Oncol 15:1844–1852.

Horwich A, Sleijfer DT, Fossa SD, Kaye SB, Oliver RT, Cullen MH, Mead GM, de Wit R, de Mulder PH, Dearnaley DP, Cook PA, Sylvester RJ, Stenning SP. 1997. Randomized trial of bleomycin, etoposide, and cisplatin compared with bleomycin, etoposide, and carboplatin in good-prognosis metastatic nonseminomatous germ cell cancer: A Multiinstitutional Medical Research Council/European Organization for Research and Treatment of Cancer Trial. J Clin Oncol 15:1844–1852.

Kataoka K, Kwon GS, Yokoyama M, Okano T, Sakurai Y. 1993. Block copolymer micelles as vehicles for drug delivey. J Controlled Release 24:119–132.

Kato K, Hamaguchi T, Matsumura Y, Yasui H, Okusaka T, Ueno H, Ikeda M, Muro K, Shirao K, Shimada Y. 2018. Phase I study of NK105, polymer micelle paclitaxel, in patients with advanced cancer. Proc Am Soc Clin Oncol 25:2006.

Khayat D, Antoine EC, Coeffic D. 2000. Taxol in the management of cancers of the breast and the ovary. Cancer Invest 18: 242–260.

Koizumi F, Kitagawa M, Negishi T, et al. 2006. Novel SN-38-incorporating polymeric micelles, NK012, eradicate vascular endothelial growth factor-secreting bulky tumors. Cancer Res 66:10048–10056.

Li LH, Fraser TJ, Olin EJ, Bhuyan BK. 1972. Action of camptothecin on mammalian cells in culture. Cancer Res 32: 2643–2650.

Matsumura Y, Maeda H. 1986. A new concept for macromolecular therapeutics in cancer chemotherapy: Mechanism of tumoritropic accumulation of proteins and the antitumor agent smancs. Cancer Res 46:6387–6392.

Muggia FM, Creaven PJ, Hansen HH, Cohen MH, Selawry OS. 1972. Phase I clinical trial of weekly and daily treatment with camptothecin (NSC-100880): Correlation with preclinical studies. Cancer Chemother Rep 56:515–521.

Nakajima T, Matsumura Y. 2007. Abstr 4729 Synergictic antitumor activity of novel polymeric micelles incorporating SN-38(NK102) in combination with 5-fluorouracil (5-FU) in mouse model of colon cancer. Proc Am Assoc Cancer Res 98.

Negoro S, Masuda N, Takada Y, Sugiura T, Kudoh S, Katakami N, et al. 2003. CPT-11 Lung Cancer Study Group West. Randomised phase III trial of irinotecan combined with cisplatin for advanced non-small-cell lung cancer. Br J Cancer 88: 335–341.

Nishiyama N, Okazaki S, Cabral H, Miyamoto M, Kato Y, Sugiyama Y, Nishio K, Matsumura Y, Kataoka K. 2003. Novel cisplatin-incorporated polymeric micelles can eradicate solid tumors in mice. Cancer Res 63:8977–8983.

Noda K, Nishiwaki Y, Kawahara M, Negoro S, Sugiura T, Yokoyama A, et al. 2002. Irinotecan plus cisplatin compared with etoposide plus cisplatin for extensive small-cell lung cancer. N Engl J Med 346:85–91.

Pinzani V, Bressolle F, Haug IJ, Galtier M, Blayac JP, Balmes P. 1994. Cisplatin-induced renal toxicity and toxicity-modulating strategies: A review. Cancer Chemother Pharmacol 35:1–9.

Roth BJ. 1996. Chemotherapy for advanced bladder cancer. Semin Oncol 23:633–644, Screnci D, McKeage MJ, Galettis P, Hambley TW, Palmer BD and Baguley BC (2000). Relationships between hydrophobicity, reactivity, accumulation and peripheral nerve toxicity of a series of platinum drugs. Br J Cancer, 82, 966–72.

Rothenberg ML, Kuhn JG, Burris HA, 3rd, Nelson J, Eckardt JR, Tristan-Morales M, et al. 1993. Phase I and pharmacokinetic trial of weekly CPT-11. J Clin Oncol 11:2194–2204.

Rowinsky EK, Donehower RC. 1995. Paclitaxel (taxol). N Engl J Med 332:1004–1014, Savic R, Luo L, Eisenberg A, Maysinger D (2003). Micellar nanocontainers distribute to defined cytoplasmic organelles. Science, 300, 615–8.

Rowinsky EK, Chaudhry V, Forastiere AA, Sartorius SE, Ettinger DS, Grochow LB, Lubejko BG, Cornblath DR, Donehower RC. 1993. Phase I and pharmacologic study of paclitaxel and cisplatin with granulocyte colony-stimulating factor: Neuromuscular toxicity is dose-limiting. J Clin Oncol 11:2010–2020.

Saltz LB, Cox JV, Blanke C, Rosen LS, Fehrenbacher L, Moore MJ, et al. 2000. Irinotecan plus fluorouracil and leucovorin for metastatic colorectal cancer. Irinotecan Study Group. N Engl J Med 343:905–914.

Saltz LB, Douillard JY, Pirotta N, et al. 2001. Irinotecan plus fluorouracil/leucovorin for metastatic colorectal cancer: A new survival standard. Oncologist 6:81–91.

Slatter JG, Schaaf LJ, Sams JP, Feenstra KL, Johnson MG, Bombardt PA, et al. 2000. Pharmacokinetics, metabolism, and excretion of irinotecan (CPT-11) following I.V. infusion of [(14)C]CPT-11 in cancer patients. Drug Metab Dispos 28: 423–433.

Takimoto CH, Arbuck SG. 2001. Topoisomerase I targeting agents: The camptothecins. In: Chabner BA, Lango DL, editors. Cancer chemotherapy and biotherapy: Principal and practice. 3rd ed., Philadelphia (PA): Lippincott Williams & Wilkins. p 579–646.

Uchino H, Matsumura Y, Negishi T, Koizumi F, Hayashi T, Honda T, et al. 2005. Cisplatin-incorporating polymeric micelles (NC-6004) can reduce nephrotoxicity and neurotoxicity of cisplatin in rats. Br J Cancer 93:678–687.

Wasserheit C, Frazein A, Oratz R, Sorich J, Downey A, Hochster H, Chachoua A, Wernz J, Zeleniuch-Jacquotte A, Blum R, Speyer J. 1996. Phase II trial of paclitaxel and cisplatin in women with advanced breast cancer: An active regimen with limiting neurotoxicity. J Clin Oncol 14:1993–1999.

Weiss RB, Donehower RC, Wiernik PH, Ohnuma T, Gralla RJ, Trump DL, Baker JR, Jr, Van Echo DA, Von Hoff DD, Leyland-Jones B. 1990. Hypersensitivity reactions from taxol. J Clin Oncol 8:1263–1268.

Yokoyama M, Miyauchi M, Yamada N, Okano T, Sakurai Y, Kataoka K, Inoue S. 1990. Polymer micelles as novel drug carrier: Adriamycin-conjugted poly(ethylene glycol)-poly(aspartic acid) block copolymer. J Controlled Release 11:269–278.

Yokoyama M, Okano T, Sakurai Y, Ekimoto H, Shibazaki C, Kataoka K. 1991. Toxicity and antitumour activity against solid tumours of micelle-forming polymeric anticancer drug and its extremely long circulation in blood. Cancer Res 51:3229–3236.

Yokoyama M, Okano T, Sakurai Y, Ekimoto H, Shibazaki C, Kataoka K. 1991. Toxicity and antitumour activity against solid tumours of micelle-forming polymeric anticancer drug and its extremely long circulation in blood. Cancer Res 51:3229–3236.

Yokoyama M, Okano T, Sakurai Y, Ekimoto H, Shibazaki C, Kataoka K. 1991. Toxicity and antitumor activity against solid tumors of micelle-forming polymeric anticancer drug and its extremely long circulation in blood. Cancer Res 51:3229–3236.